

# 1 Raman characterization of synthetic magnesian calcites

## 2 Revision\_2

3 Jonathan Perrin<sup>a1</sup>, Daniel Vielzeuf<sup>a</sup>, Didier Laporte<sup>b</sup>, Angèle Ricolleau<sup>a</sup>, George R Rossman<sup>c</sup>,  
4 Nicole Floquet<sup>a</sup>

5 <sup>a</sup> Aix-Marseille Université, CNRS, CINaM UMR7325, 13288, Marseille, France

6 <sup>b</sup> Laboratoire Magmas et Volcans, Université Blaise Pascal – CNRS - IRD, OPGC, 5 rue  
7 Kessler, 63038 Clermont-Ferrand, France

8 <sup>c</sup> Division of Geological and Planetary Sciences, California Institute of Technology,  
9 Pasadena, CA 91125-2500, USA

10  
11

## 12 Contents

13	<b>1 Introduction.....</b>	<b>3</b>
14	<b>2 Materials and methods .....</b>	<b>4</b>
15	2.1 Experimental syntheses.....	4
16	2.2 Analytical methods .....	5
17	<b>3 Results .....</b>	<b>7</b>
18	3.1 Calcite, magnesite and dolomite optically clear natural (OCN) crystals .....	7
19	3.2 Synthetic Mg calcites .....	9
20	3.2.1 MEB and EMP characterization.....	9
21	3.2.2 The effect of Mg incorporation on synthetic Mg calcite Raman bands .....	11
22	<b>4 Discussion .....</b>	<b>14</b>
23	4.1 Comparison with previous works .....	14
24	4.2 Structural interpretation .....	15
25	4.2.1 Raman shifts .....	15
26	4.2.2 FWHM of Raman bands .....	17
27	4.3 Comparison with magnesian amorphous calcium carbonate .....	19
28	<b>5 Implications.....</b>	<b>20</b>
29	<b>Acknowledgments.....</b>	<b>20</b>
30	<b>Bibliography.....</b>	<b>24</b>

31  
32  
33

---

<sup>1</sup> **Corresponding author** J. Perrin. Address: CNRS, UMR7325, Aix-Marseille Université, CINaM, 13288, Marseille, France. E-mail addresses : [perrin@cinam.univ-mrs.fr](mailto:perrin@cinam.univ-mrs.fr) (J. Perrin), [vielzeuf@cinam.univ-mrs.fr](mailto:vielzeuf@cinam.univ-mrs.fr) (D. Vielzeuf), [D.Laporte@opgc.univ-bpclermont.fr](mailto:D.Laporte@opgc.univ-bpclermont.fr) (Didier Laporte), [ricolleau@cinam.univ-mrs.fr](mailto:ricolleau@cinam.univ-mrs.fr) (A. Ricolleau), [grr@gps.caltech.edu](mailto:grr@gps.caltech.edu) (George Rossman), [floquet@cinam.univ-mrs.fr](mailto:floquet@cinam.univ-mrs.fr) (N. Floquet).

34

### Abstract

35 *Magnesian calcites are important components of sediments and biominerals. Although*  
36 *Raman spectra of calcite, dolomite, and magnesite are well known, those of magnesian*  
37 *calcites deserve further investigation. Nineteen syntheses of magnesian calcites covering the*  
38 *range 0-50 mol% MgCO<sub>3</sub> have been carried out at high pressure and temperature (1-1.5*  
39 *GPa, 1000-1100°C). The crystalline run products have been characterized by μ-Raman*  
40 *spectroscopy.*

41 *For all lattice and internal modes (L, T, v<sub>1</sub>, v<sub>4</sub>, 2v<sub>2</sub>) but v<sub>3</sub>, wavenumbers align closer*  
42 *to the calcite–dolomite line than the calcite–magnesite line. The compositional dependence is*  
43 *strong and regression curves with high correlation coefficients have been determined. Full*  
44 *width at half maximum (FWHM) plot along parabolas that depart from the calcite–dolomite*  
45 *or calcite–magnesite lines. The limited data dispersion of both shifts and FWHM allow using*  
46 *Raman spectral properties of magnesian calcites to determine the Mg content of abiotic*  
47 *calcites.*

48 *A comparison with Raman data from the literature obtained on synthetic magnesian*  
49 *amorphous calcium carbonate (Mg ACC) shows that the wavenumber position of the ACC v<sub>1</sub>*  
50 *mode is systematically shifted towards lower values, and that their FWHM are higher than*  
51 *those of their crystalline counterparts. The FWHM parameters of crystalline and amorphous*  
52 *materials do not overlap, which allows a clear-cut distinction between crystalline and*  
53 *amorphous materials.*

54 *In synthetic magnesian calcites, the shift and FWHM of Raman bands as a function of*  
55 *magnesium can be interpreted in terms of changes of metal-O bond lengths resulting from the*  
56 *replacement of calcium by magnesium. The facts that the wavenumber of magnesian calcites*  
57 *are close to the calcite–dolomite line (not calcite–magnesite), that the FWHM of the T, L, and*  
58 *v<sub>4</sub> modes reach a maximum around 30±5 mol% MgCO<sub>3</sub>, and that a peak specific to dolomite*  
59 *at 880 cm<sup>-1</sup> is observed in high-magnesian calcites indicate that dolomite-like ordering is*  
60 *present above ~10 mol% MgCO<sub>3</sub>. Mg atom clustering in cation layers combined with*  
61 *ordering in successive cation basal layers may account for the progressive ordering observed*  
62 *in synthetic magnesian calcites.*

63

64

65

66

## Introduction

67 Calcite is the only  $\text{CaCO}_3$  crystalline polymorph that can accommodate substantial amounts  
68 of magnesium (Bischoff et al., 1983; Finch and Allison, 2007; Long et al., 2012; Mackenzie  
69 et al., 1983; Morse et al., 2007; Wang et al., 2012). Magnesian calcites (Mg calcites) are  
70 important components of modern and Pleistocene carbonate sediments (Bischoff et al., 1985;  
71 Land, 1967). In the sediments, they are mostly found as remnants of skeletons of marines  
72 invertebrates and as cement (Bathurst, 1975; Bischoff et al., 1985; Chave, 1954a; Chave,  
73 1954b). Since Raman spectroscopy is sensitive to carbonate ion ( $\text{CO}_3^{2-}$ ) vibrations, micro-  
74 Raman spectroscopy is classically used to characterize small volumes of crystalline or  
75 amorphous carbonate samples. Raman patterns of the different calcium carbonate polymorphs  
76 (calcite, aragonite, vaterite, amorphous calcium carbonate) are well identified; however, the  
77 Raman spectral modifications due to variations of chemical composition are less known. The  
78 effect of magnesium incorporation in calcite has been thoroughly investigated by Bischoff et  
79 al. (1985). These authors characterized the wavenumber shifts and enlargements of the  
80 carbonate vibration modes in magnesian calcites as a function of their Mg contents. Carbonate  
81 vibration modes of calcite (Cal:  $\text{CaCO}_3$ ), dolomite (Dol:  $\text{Ca}_{0.5}\text{Mg}_{0.5}\text{CO}_3$ ) and magnesite (Mgs:  
82  $\text{MgCO}_3$ ) show a shift toward higher wavenumber and enlargement as a function of  
83 magnesium content. Bischoff et al. (1985) also showed that magnesian calcites display  
84 changes of spectral properties aligned along the calcite-magnesite line with slightly positive  
85 or negative deviations from linearity for  $\nu_3$  and the translational T modes. The full widths at  
86 half maximum (FWHM) of the vibrational Raman bands progressively increase as a function  
87 of magnesium contents. However, according to these authors, the shift and FWHM data  
88 dispersions are too large to allow the determination of calcite Mg contents from their Raman  
89 properties. In particular, the Raman shift of the 25 mol%  $\text{MgCO}_3$  sample [i.e. the highest  
90 magnesium content studied by Bischoff et al. (1985)] diverges from the general tendency.

91 Additional data are needed to clarify these points. In the present study, micro-Raman data  
92 obtained on a new series of magnesian calcites synthesized at high pressure and temperature  
93 are presented.

94 Amorphous calcium carbonates (ACC) are widespread in biomineralizing  
95 environments, and the formation and transformation of this intermediate and reactive phase  
96 are new centers of interest in the biomineralization community (Addadi et al., 2003; Beniash  
97 et al., 1997; Benzerara et al., 2006; Politi et al., 2004; Politi et al., 2006; Tao et al., 2009;  
98 Wang et al., 2009; Weiner et al., 2005; Weiss et al., 2002). A recent study dealing with the  
99 experimental synthesis of ACC with variable magnesium contents (0 to 43 mol% MgCO<sub>3</sub>)  
100 showed that Raman spectroscopy can be used to determine magnesium contents of ACC  
101 (Wang et al., 2012). Indeed, both the position and the FWHM of the fundamental band  $\nu_1$  of  
102 ACC are linear functions of magnesium content. Below, the data obtained on newly  
103 synthesized magnesian calcites will be compared with the data obtained by Wang et al. (2012)  
104 to better understand the changes of Raman properties of calcium carbonates as their Mg  
105 contents and structure change.

## 106 **Materials and methods**

### 107 **Experimental syntheses**

108 Nineteen magnesian calcites have been synthesized in the range 2-50 mol% MgCO<sub>3</sub> at high  
109 pressure and high temperature in a piston-cylinder apparatus. The starting material for our  
110 synthesis experiments consists of pure synthetic calcite (Alfa Aesar) and natural magnesite  
111 from Brumado (Bahia, Brazil). ICP-AES analyses of magnesite indicate trace amounts of Fe  
112 (0.15 wt% Fe<sub>2</sub>O<sub>3</sub>) and Ca (0.22 wt% CaO). The magnesite was ground in a McCrone  
113 micronizer agate mortar in ethanol for 30 min. Calcite and magnesite were mixed in  
114 appropriate molar proportions and manually ground in an agate mortar with ethanol. After



139 close to 100 was taken as an indication of a good analysis. Throughout this article, the  
140 compositions of magnesian calcites are expressed in mol% MgCO<sub>3</sub>.

141 *Micro-Raman spectroscopy* - Samples were analyzed on a Renishaw M-1000 Micro-Raman  
142 spectrometer operating with a 514.5 nm argon ion laser, at a spectral resolution of 1 cm<sup>-1</sup>. A  
143 dual-wedge polarization scrambler inserted directly above the objective lens was used to  
144 minimize polarization effects. A spot size of about 1 μm was used to respond to spatial  
145 constraints associated with the size of the synthetic crystals (100-200 μm). Analytical  
146 conditions were chosen to optimize signal to noise ratio: usually 10 scans per spectrum, 10 s  
147 per wavelength on the detector, 100% power and a 20 μm slit. Spectral peak positions were  
148 periodically calibrated against a silicon standard (at 520.5 cm<sup>-1</sup>) and rarely varied more than 1  
149 cm<sup>-1</sup>. The additional measurements in the range 650-950 cm<sup>-1</sup> presented in the Fig. 9 (inset)  
150 were carried out at LMV (Clermont-Ferrand – France) on a Renishaw InVia Micro Raman  
151 spectrometer operating with a 532 nm argon ion laser. Analyses were carried out at a spectral  
152 resolution of 1 cm<sup>-1</sup>, in extended mode, with high confocality, 10% power, 10 scans per  
153 spectrum, and 15 s exposure time. Spectral peak positions were also calibrated against a  
154 silicon standard. All micro-Raman analyses were carried out on polished samples mounted in  
155 epoxy. No additional sample preparation was needed for the Raman measurements. Whenever  
156 possible, μ-Raman analyses were made on, or close to grains analyzed by electron microprobe  
157 (EMP). Spot positioning was made using the 100× magnification lens on the microscope. The  
158 Renishaw Wire software (<http://www.renishaw.fr/wire>) was used for background removal and  
159 wavenumber determination, while Winplotr (Roisnel and Rodríguez-Carvajal, 2001) was used  
160 for peak FWHM determinations.

161

162

## Results

163

### Calcite, magnesite and dolomite optically clear natural (OCN) crystals

164 Carbonates have six vibration modes composed of two external (or lattice) modes and four  
165 internal modes (Couture, 1947; White, 1974a). Different notations are used in the literature to  
166 refer to these vibration modes; they are listed in **Table 1** with a brief description of their  
167 physical significance. For clarity, the following notation initially used by Cabannes and  
168 Aynard (1942), Couture (1947), Kastler and Rousset (1941) and also by Bischoff et al. (1985)  
169 will be used throughout the text: translational (T) and librational (rotatory) (L) external  
170 modes;  $\nu_1$ ,  $\nu_2$ ,  $\nu_3$  et  $\nu_4$  internal modes. The notation derived from factor group theory (see  
171 **Table 1**) will be associated to the previous notation only when necessary. The internal  
172 vibrations  $\nu_1$ ,  $\nu_2$ ,  $\nu_3$  and  $\nu_4$  involve bending or stretching of the C-O bonds in the carbonate  
173 groups in and out of the plane in the  $a$  direction (Bhagavantam and Venkatarayudu, 1939;  
174 Krishnan, 1945). Importantly, group theory shows that some silent Raman modes that cannot  
175 be found in the first-order spectrum of a crystal can be observed in the second-order spectrum  
176 (Dresselhaus et al., 2008). For instance, in calcite and magnesite,  $\nu_2$  (at  $\sim 880 \text{ cm}^{-1}$ ) is Raman  
177 silent while its overtone  $2\nu_2$  (at  $\sim 1760 \text{ cm}^{-1}$ ) is observed (Couture, 1947). The external  
178 vibrations (T and L) involve relative translations of the metal (e.g.  $\text{Ca}^{2+}$  or  $\text{Mg}^{2+}$ ) and  $\text{CO}_3^{2-}$   
179 ions and librations of  $\text{CO}_3^{2-}$  ions (Couture, 1947). Band assignments of lattice modes (L or T)  
180 are equivocal, probably as a consequence of mixing (Bischoff et al., 1985). Nevertheless, the  
181 notation used by Bischoff et al. (1985) (T:  $[155\text{-}212 \text{ cm}^{-1}]$ ; L:  $[282\text{-}331 \text{ cm}^{-1}]$ ) will be used for  
182 the sake of simplicity.

183 The positions of the six active Raman modes in calcite, dolomite and magnesite OCN  
184 crystals are displayed in **Fig. 1** and **Table 2**. The doubly degenerate lattice modes T and L and  
185 the three internal modes  $\nu_4$ ,  $\nu_3$  and  $2\nu_2$  show a shift toward high wavenumbers from calcite to  
186 magnesite, i.e. as Mg increases (**Fig. 1**). However, this systematic effect is not observed in the

187 non-degenerated  $\nu_1$  internal mode, which is less shifted in magnesite than in dolomite. These  
188 observations are in agreement with the previous measurements of Bischoff et al. (1985) and,  
189 at least qualitatively with the calculated values of Schauble et al. (2006) using density  
190 functional perturbation theory. The singular behavior of  $\nu_1$  could be due to the fact that this  
191 mode is related to a  $\text{CO}_3^{2-}$  in-plane vibration (stretch) with little Ca-Mg cation involvement  
192 (Boulard et al., 2012).

193 It has been established for a long time that the crystallographic symmetry of dolomite (R-  
194 3) is lower than that of calcite and magnesite (R-3c) due to alternating layers of Ca and Mg in  
195 dolomite. As a consequence, a weak additional peak lattice mode at  $\sim 335 \text{ cm}^{-1}$  is observed in  
196 dolomite (Bischoff et al., 1985). In most dolomite Raman spectra listed in the online Ruff  
197 database (<http://rruff.info/Dolomite>), as in Fig. 1 (inset a), this peak is close to the T mode  
198 band and can be easily overlooked. Various authors (Couture, 1947; Schauble et al., 2006;  
199 Valenzano et al., 2007) also noted that two Raman-active  $A_g$  modes in dolomite (at 231 and  
200  $876 \text{ cm}^{-1}$ ) are related to inactive  $A_{2g}$  modes in calcite and magnesite. These peaks should be  
201 observed in dolomite and not in calcite or magnesite. However, according to Schauble et al.  
202 (2006) these peaks would be too weak to be distinguished from experimental background  
203 noise. This observation is verified for the  $231 \text{ cm}^{-1}$  peak that has not been observed in any  
204 published Raman spectra (to our knowledge). On another hand, our measurements on the  
205 OCN dolomite show the presence of a sharp peak at  $881 \text{ cm}^{-1}$  well above background noise.  
206 This peak is also observed in six dolomites referenced in the Ruff database, in particular  
207 those from Bay Mag mine (British Columbia, Canada) and Oberdorf (Austria). Below,  
208 particular attention will be paid to this  $\nu_2$  mode at  $\sim 880 \text{ cm}^{-1}$  which can be taken as an  
209 indicator of dolomite-like ordering in Mg calcites. The structural difference between  
210 calcite/magnesite on one side, and dolomite on the other side, led Bischoff et al. (1985) to  
211 consider that calcite and magnesite were the actual end members of the Mg calcite solid



212 solution, and thus that the spectral properties of Mg calcites should plot between calcite and  
213 magnesite (the calcite-magnesite line) and not between calcite-dolomite. This is an important  
214 conclusion that has to be verified.

215 Concerning the FWHM, **Fig. 1** and **Table 2** indicate that the peak widths of the T and L  
216 lattice modes progressively decrease from calcite to magnesite (as Mg increases) while those  
217 of the internal  $\nu_1$  and  $\nu_4$  modes increase. The situation is more complex regarding  $\nu_3$  and  $2\nu_2$   
218 since their FWHM increase from calcite to dolomite, then decrease slightly (or stay constant)  
219 from dolomite to magnesite (**Fig. 1** and **Table 2**). Our FWHM determinations for the T, L,  $\nu_1$   
220 and  $\nu_4$  modes are in agreement with those of Bischoff et al. (1985), within  $\pm 1 \text{ cm}^{-1}$  which is  
221 the instrument resolution. This is not the case for the  $\nu_3$  and  $2\nu_2$  modes that show higher  
222 FWHM than those determined by Bischoff et al. (1985). These differences could be due to  
223 larger error margins associated with low peak intensities and background removal processing.

224

### Synthetic Mg calcites

225

#### MEB and EMP characterization

226 High pressure and high temperature experimental products were extracted from the gold  
227 capsule as friable grey to white blocks of Mg calcite crystals. The grey color of some run  
228 products comes from a small fraction of graphite. Some SEM images of the run products are  
229 shown in **Fig 2**. Crystals display polyhedral shapes and have sizes in the range 100-200  $\mu\text{m}$   
230 (**Fig. 2c, d**). Numerous grain triple junctions at  $120^\circ$  indicative of textural equilibrium are  
231 observed (**Fig. 2b**). In almost all experiments, small empty spaces are found between Mg  
232 calcite grains (**Fig. 2c, d**). These voids are interpreted as pores containing a low density fluid  
233 phase. Traces of carbonate melt evidenced by quench crystals (usually against the gold  
234 capsule) are observed in most experiments. They are attributed to small amounts of adsorbed  
235 water in the starting material that lead to incipient melting at temperatures below the solidus  
236 for the dry system. In one experiment (MgCc\_45) carried out at  $1100^\circ\text{C}$  and 1.5 GPa, the

237 proportion of melt was important as about half of the capsule was occupied by 1-2 mm long  
238 quench crystals, well segregated from polyhedral crystals in the other half of the capsule.  
239 These features indicate that the solidus was overstepped in this experiment. This is in fairly  
240 good agreement with the phase diagrams published on the system  $\text{CaCO}_3\text{-MgCO}_3$  (Goldsmith  
241 and Heard, 1961; Irving and Wyllie, 1975). For micro-Raman acquisitions, zoned quench  
242 crystals were avoided and analyses were carried out on polyhedral crystals. The Mg contents  
243 of magnesian calcites determined by EMP are plotted against nominal compositions in Fig. 3.  
244 The measured compositions are systematically slightly lower than expected. The difference  
245 between nominal and measured values increases from low to high Mg contents, at least up to  
246 35 mol%  $\text{MgCO}_3$ . This systematic composition shift can be attributed to limited  
247 decarbonation of magnesite taking place during the heating stage at the beginning of the  
248 experiment. This interpretation is consistent with the presence of pores between grains (these  
249 pores being probably filled with  $\text{CO}_2$ ). At 35 mol%  $\text{MgCO}_3$ , two different crystal  
250 compositions coexist in the same capsule ( $28.3 \pm 0.3$  and  $33.3 \pm 0.2$  mol%  $\text{MgCO}_3$ ). This  
251 situation is attributed to the presence of a solvus between calcite and dolomite (Byrnes and  
252 Wyllie, 1981).

253 The quality of the synthetic crystals was determined by conventional X-ray diffraction.  
254 No  $\text{CaCO}_3$  polymorph other than calcite (aragonite or vaterite) was detected. Powder XRD  
255 data obtained on a high flux X-ray synchrotron beamline will be presented in a companion  
256 paper. In the present article dedicated to micro-Raman spectroscopy, two groups of  
257 experiments corresponding to the 0-30 and 35-50 mol%  $\text{MgCO}_3$  composition ranges will be  
258 distinguished. This partition is justified by different facts: (1) most biominerals have Mg  
259 contents in the range 0-30 mol%  $\text{MgCO}_3$ . For this reason, particular emphasis was put on this  
260 compositional range with syntheses carried out at a 2 mol%  $\text{MgCO}_3$  step interval. For more  
261 magnesian compositions of lower practical interest for biominerals, a 5 mol%  $\text{MgCO}_3$  step

262 interval was used to minimize the number of experiments. (2) Phase diagrams indicate that  
263 due to the presence of a miscibility gap between calcite and dolomite, higher P and T are  
264 required to synthesize Mg calcites in the range 35-50 mol% MgCO<sub>3</sub> (1.5 GPa, 1100°C instead  
265 of 1 GPa and 1000°C). Thus, different experimental conditions were used for the two sets of  
266 experiments. Furthermore, phase relationships are more complicated in the high Mg field with  
267 possibility of unmixing and partial melting (see Byrnes and Wyllie, 1981 for a review). (3)  
268 Finally, the behavior of the solid solution above 30 mol% MgCO<sub>3</sub> is more complex than  
269 within the range 0-30 mol% MgCO<sub>3</sub>, and shows more dispersion in the analytical results.

### 270 **The effect of Mg incorporation on synthetic Mg calcite Raman bands**

#### 271 **The 0-30 mol% MgCO<sub>3</sub> composition range**

272 The Raman spectra of synthetic calcites show decreasing intensities of the different modes as  
273 Mg increases as shown on three MgCO<sub>3</sub> compositions in Fig. 4. This effect is important even  
274 at low Mg contents: for instance, the T, L and  $\nu_1$  intensities of the 3.2 mol% MgCO<sub>3</sub> calcite  
275 are about half those of the OCN calcite crystal. As Mg increases, the six Raman carbonate  
276 bands show both progressive shifts towards high wavenumbers, and peak enlargements.  
277 Normalized intensities after baseline extraction allow a precise analysis of the band shifts and  
278 enlargements. Table 3 summarizes the positions and FWHM of the Raman bands for all  
279 synthetic magnesian calcites. Figure 5 shows the position of the main active Raman modes as  
280 a function of magnesium contents between 2 and 30 mol% MgCO<sub>3</sub>. The  $\nu_3$  mode shows a  
281 large dispersion that cannot be attributed to instrumental error but to a strong decrease of peak  
282 intensity as Mg enters the structure. For all other modes, the wavenumbers as a function of  
283 magnesium content are well aligned and can be adjusted with third degree polynomial  
284 functions with excellent correlation coefficients ( $R^2 > 0.98$ ) (see Table 3). A third degree  
285 polynomial has been selected to have a better fit and also because the observed curvatures are  
286 considered experimentally meaningful. However, a simple linear function would also fit the

287 data correctly (as we will see later when the complete composition range is considered). In  
288 most cases (T, L and  $\nu_1$ ), the data are closer to the calcite-dolomite line than to calcite-  
289 magnesite. In addition, a significant negative deviation from the calcite-dolomite line is also  
290 observed at least up to 20 mol%  $\text{MgCO}_3$ . The fact that the wavenumber of the  $2\nu_2$  mode is  
291 closer to Cal-Mgs than Cal-Dol could be attributed to such a negative deviation from Cal-Dol  
292 and not to an alignment along Cal-Mgs. **Table 4** summarizes the parameters and the  
293 correlation coefficients of the regression curves shown in **Fig. 5**. To summarize, in the range  
294 0-30 mol%  $\text{MgCO}_3$ , the wavenumber of all modes except  $\nu_3$  are well aligned with slightly  
295 negative deviations with respect to the Cal-Dol line.

296       Concerning the FWHM, **Fig. 6** emphasizes the systematic peak enlargement as Mg  
297 increases. However, the FWHM of the T mode reach a plateau at about 25 mol%  $\text{MgCO}_3$  with  
298 an inversion of slope above this value. The normalized FWHM align along 2<sup>nd</sup> order  
299 polynomial curves. The regression curves of the L and  $\nu_4$  FWHM have correlation  
300 coefficients greater than 0.99. All parameters and correlation coefficients of the regression  
301 curves are listed in **Table 4**.

### 302                                   **The 35-50 mol% $\text{MgCO}_3$ composition range**

303 **Figure 7** presents the positions of the vibration modes of Mg calcites synthesized between 35  
304 and 50 mol%  $\text{MgCO}_3$ . Data from the 0-30 mol%  $\text{MgCO}_3$  range are also plotted for  
305 comparison. The position of the modes in the 35-50 mol%  $\text{MgCO}_3$  range follows the trend  
306 defined earlier. However, the data dispersion is greater, in particular for the L,  $\nu_1$  and  $2\nu_2$   
307 modes. As observed within the 0-30 mol%  $\text{MgCO}_3$  composition range, the shifts of the  $\nu_3$   
308 mode do not show proper alignment due to very weak intensities. In all other modes and  
309 without ambiguity, even for the  $2\nu_2$  overtone, the data are closer to the Cal-Dol line than to  
310 the Cal-Mgs line. Although the two datasets were obtained under different P and T conditions,  
311 the data generate linear regressions with high correlation coefficients (>0.98). These

312 regressions are valid within the range 0-50 mol% MgCO<sub>3</sub>. The best correlation coefficients  
313 (>0.99) are obtained for the T, L and v<sub>4</sub> modes (Table 5).

314 The FWHM of the synthetic Mg calcites in the range 35-50 mol% MgCO<sub>3</sub> are shown  
315 in Fig. 8. Again, data from the 0-30 mol% MgCO<sub>3</sub> composition range are plotted for  
316 comparison. These data confirm the incipient change of slope observed in Fig. 6a for the T  
317 mode; they also show that a change of slope is observed for the L and v<sub>4</sub> modes (and possibly  
318 v<sub>3</sub> and 2v<sub>2</sub>). The data of the T, L, v<sub>4</sub> and 2v<sub>2</sub> modes can be fit with a 2<sup>nd</sup> order polynomial  
319 function valid within the range 0-50 mol% MgCO<sub>3</sub>. The L and v<sub>4</sub> modes present the best  
320 correlation coefficients (R<sup>2</sup> >0.98). Note that regressions for the entire 0-50 mol% MgCO<sub>3</sub>  
321 range are proposed to emphasize the consistency of the data. However, for applications in the  
322 0-30 mol% MgCO<sub>3</sub> range, the regressions listed in Table 4 should be preferred. The maxima  
323 of the fitting parabola are reached for Mg contents of 25, 30, and 35 mol% MgCO<sub>3</sub> for the T,  
324 L, and v<sub>4</sub> modes, respectively. However, as a word of caution, it should be reminded that the  
325 two datasets plotted in Fig. 8 were obtained from crystals synthesized under different  
326 temperatures, a critical parameter for crystal ordering, and thus FWHM. Nevertheless, the  
327 inversion of slope suspected in Fig. 6 and confirmed in Fig. 8 remains a robust observation  
328 that has to be considered to interpret the data. Concerning the v<sub>3</sub> mode, considering the poor  
329 alignment of the wavenumber as a function of Mg content (Fig. 7e), the FWHM displayed in  
330 Fig. 8e are rather well organized even if the data dispersion is greater above 30 mol% MgCO<sub>3</sub>;  
331 here again, a change of slope can be suspected at about 30-35 mol% MgCO<sub>3</sub>. For the 2v<sub>2</sub>  
332 mode, the change of slope is not observed at 30 mol% MgCO<sub>3</sub>, but could be present at 50  
333 mol% MgCO<sub>3</sub>. Because of the large data dispersion at high Mg contents and the lack of  
334 experiment above 50 mol% MgCO<sub>3</sub>, this conclusion has to be confirmed. The FWHM of the  
335 v<sub>1</sub> mode deserves further consideration since the data cannot be properly fit with a quadratic  
336 function (Fig. 8d). Indeed, the change of slope observed at about 30 mol% MgCO<sub>3</sub> (Fig. 8d) is

337 due to peak doubling (Fig. EA1) that becomes obvious at 30 mol% MgCO<sub>3</sub>. Two different  
338 ways to fit the  $\nu_1$  band with one and two peaks are presented and discussed in supplementary  
339 data EA1.

340 In paragraph 3.1, the importance of two peaks that are specific to dolomite (at 340 and  
341 880 cm<sup>-1</sup>) has been emphasized. An important question is whether these peaks are observed in  
342 the synthetic Mg calcites. Not much can be said about the peak located at 340 cm<sup>-1</sup> as the shift  
343 towards high wavenumbers and broadening of the adjacent L peak render the observation of  
344 this peak difficult. Nevertheless, a significant signal is detected in crystals with 49.2 mol%  
345 MgCO<sub>3</sub>. On another hand,  $\nu_2$  at ~880 cm<sup>-1</sup> should be easier to detect as it is not concealed by  
346 any neighbor. Figure 9 shows Raman spectra of all experimental products in the range 840-  
347 920 cm<sup>-1</sup>. It shows that the 880 cm<sup>-1</sup> peak is absent at low Mg contents and progressively  
348 appears as Mg increases. In this series of measurements, the first experiment at which the  
349 peak can be identified with confidence is 18.2 mol% MgCO<sub>3</sub>. A second series of micro-  
350 Raman analyses of the magnesian calcites with MgCO<sub>3</sub> contents up to 14.5 mol% MgCO<sub>3</sub> was  
351 carried out in the restricted 650-950 cm<sup>-1</sup> range, with longer exposure time to improve the  
352 signal/noise ratio. Results are presented in the inset of Fig. 9. These data show that the 880  
353 cm<sup>-1</sup> peak can be identified down to 9.7 (and possibly 6.1) mol% MgCO<sub>3</sub>. A slight shift of this  
354 peak towards high wavenumbers is also observed as Mg increases.

## 355 Discussion

### 356 Comparison with previous works

357 The shifts of vibration modes toward high wavenumbers as a function of Mg content can be  
358 compared to those of Bischoff et al. (1985) (Fig. 7). If the experiment at 25 mol% MgCO<sub>3</sub> of  
359 Bischoff et al. (1985) is discarded, the wavenumber shifts of the L and  $\nu_4$  modes are in good  
360 agreement in both studies, though the present data are less dispersed (Fig. 7b, c). For the T,  $\nu_1$ ,  
361 and  $2\nu_2$  modes, there is no agreement: Bischoff et al. (1985) observed a weak or no

362 correlation of wavenumber positions with Mg content for these modes, while a strong Mg  
363 dependence with high coefficients of correlation is observed in our dataset (Fig. 7a, d, f).  
364 Finally, neither Bischoff et al. (1985) nor us observed a composition dependence on the  $\nu_3$   
365 wavenumber (Fig. 7e).

366 Concerning the FWHM, Fig. 8 indicates that the present results are in fairly good  
367 agreement with those of Bischoff et al. (1985) in the range 0-20 mol% MgCO<sub>3</sub> for all modes  
368 except  $\nu_3$ , even if the synthetic Mg calcite with 25 mol% MgCO<sub>3</sub> of Bischoff et al. (1985) is  
369 not on the tendency for the L mode. The data for the  $\nu_3$  mode are well aligned in both our and  
370 Bischoff et al. (1985) datasets but the slopes of the fitting curves differ (Fig. 8e). Finally, the  
371 wider range of compositions synthesized in our study indicates that a curve and not a line is  
372 required to fit the data properly. The departure from linearity could not be detected by  
373 Bischoff et al. (1985) as it occurs above 25 mol% MgCO<sub>3</sub>, the highest Mg content studied by  
374 these authors.

## 375 **Structural interpretation**

### 376 **Raman shifts**

377 The shift of Raman bands toward higher wavenumbers from calcite to magnesite OCN  
378 crystals (Fig. 1) can be attributed to the fact that the Mg<sup>2+</sup> ion is smaller than Ca<sup>2+</sup>; the Ca/Mg  
379 substitution implies a decrease of interatomic metal-O distances (2.39 Å, and 2.11 Å for the  
380 Ca-O and Mg-O bond, respectively (Politi et al., 2010; Politi et al., 2006), a variation of the  
381 cell volume and a subsequent increase of the vibrational frequencies of the carbonate ion  
382 (Krishnamurti, 1956; White, 1974a). In other words, the cation size is responsible for band  
383 displacements toward high wavenumbers as Mg increases (Rutt and Nicola, 1974; White,  
384 1974a). It should be reminded that the shift towards high wavenumbers from calcite to  
385 dolomite and then magnesite is observed for all Raman modes except one,  $\nu_1$  (Fig. 1d, see also  
386 Bischoff et al 1985, their Fig. 2) as discussed above.

387 Factor group analysis predicts that Mg calcites should have Raman spectra similar to  
388 end members but with a continual wavenumber shift between them (Bischoff et al., 1985;  
389 White, 1974b). Thus the question of the nature of the end members arises: should dolomite  
390 ( $\text{Ca}_{0.5}\text{Mg}_{0.5}\text{CO}_3$ ) or magnesite ( $\text{MgCO}_3$ ) be considered the magnesian end member of Mg  
391 calcites? From X-ray powder diffraction studies on their synthetic Mg calcites, Bischoff et al.  
392 (1983) concluded that there was no dolomite-like preferential atomic arrangement of  
393 magnesium in their synthetic Mg calcites and that the end members of the Mg calcite solid  
394 solution should be calcite/magnesite, and not calcite/dolomite. This conclusion was in  
395 agreement with previous experimental results. For instance, Goldsmith et al. (1961) stated that  
396 it is not correct to consider the region between calcite and dolomite as a simple solid solution  
397 because the dolomite structure (R-3) is ordered with respect to Ca and Mg, while the  
398 intermediate members of the solid solution have a disordered Ca-Mg array with the calcite  
399 space group R-3c. Mackenzie et al. (1983) moderated this conclusion and stated that the  
400 syntheses of Goldsmith et al. (1961) with concentrations greater than 42.5 mol%  $\text{MgCO}_3$   
401 always led to X-ray diffraction patterns showing evidence of dolomite-type cation ordering.  
402 Mackenzie et al. (1983) acknowledged the fact that there was no (101), (015) or (021)  
403 reflections in the XRD patterns of Bischoff et al.'s syntheses, probably excluding the  
404 possibility of dolomite-type cation ordering in Mg calcites. However, as a word of caution,  
405 Mackenzie et al. (1983) added that short range ordering, not necessarily detected by XRD,  
406 could account for some of the negative excess volume observed in the synthetic Mg calcites  
407 (Bischoff et al., 1983). Nevertheless, at present, the generally accepted idea as summarized by  
408 Morse et al. (2007) is that magnesium substitutes for calcium in a completely random manner  
409 in magnesian calcites. On the contrary, different facts presented here lead to the idea of a  
410 progressive ordering of Ca and Mg atoms in the cation layers: (1) the trends observed in **Figs.**  
411 **5** and **7** are closer to the Cal-Dol line than to the Cal-Mgs line. This is observed for the T, L,



412  $\nu_4$ , and  $\nu_1$  modes. (2) Peak asymmetry becomes more pronounced as peaks broaden with  
413 increasing Mg contents above 20 mol%  $\text{MgCO}_3$  (valid for all the doubly degenerate modes  
414 but also the non-degenerate  $\nu_1$  and  $2\nu_2$  modes); this could indicate that the peaks are a  
415 convolution of two discrete peaks. (3) Finally, an additional band at  $\sim 880\text{ cm}^{-1}$  corresponding  
416 to  $\nu_2$  vibration, only active in dolomite, appears in the synthetic Mg calcites at Mg contents of  
417 about 10 mol%  $\text{MgCO}_3$ , and progressively grows with increasing Mg content (Fig. 9).

### 418 **FWHM of Raman bands**

#### 419 **Calcite, dolomite, magnesite OCN crystals**

420 The FWHM of Raman bands are function of temperature, analytical conditions (spectral  
421 resolution), sample crystallinity (crystalline defects, crystallite sizes), structural disorder,  
422 substitution of trace elements, and compositional variability of the crystallites. The cation size  
423 also plays a role in the FWHM of the various modes in rhombohedral carbonates (Bischoff et  
424 al., 1985). Raman data obtained on calcite and magnesite OCN crystals provide information  
425 on the parameters controlling the FWHM of the Raman bands. The differences of FWHM of  
426 lattice and internal modes of these two minerals are function of cation size associated with  
427 difference of strength of metal-oxygen bonds. In calcite and magnesite, the length of the C-O  
428 bond in the carbonate ion is almost similar [ $1.2878\text{ \AA}$  in calcite vs  $1.2858\text{ \AA}$  in magnesite  
429 (Valenzano et al., 2007)], but the Ca-O bond in calcite is longer ( $2.39\text{ \AA}$ ), and consequently  
430 weaker, than the Mg-O bond in magnesite ( $2.11\text{ \AA}$ ). A stronger Mg-O bond means a stronger  
431 coupling between cation and carbonate group, and less frequency variation in the lattice  
432 modes (Bischoff et al., 1985). Thus, smaller FWHM of T and L modes in magnesite than in  
433 calcite are expected and observed. On the contrary, the FWHM of the internal modes  $\nu_1$ ,  $2\nu_2$ ,  
434  $\nu_3$  and  $\nu_4$  of magnesite are larger than those of calcite (Fig. 8). Again, this could be due to  
435 stronger Mg-O bonds that might have more effect on the internal vibrations of the carbonate  
436 than the weaker Ca-O bonds. Our experimental data on OCN crystals (Fig. 8, Table 2) are in

437 agreement with this interpretation initially proposed by Bischoff et al. (1985). It will be noted  
438 that the  $\nu_4$  FWHM of dolomite is close to the calcite-magnesite line (Fig. 8): most other  
439 modes display slight to relatively large positive deviations with respect to the calcite-  
440 magnesite line, except  $\nu_1$  showing a singular behavior again, and a significant negative  
441 deviation.

### 442 **Synthetic Mg calcites**

443 The FWHM of the synthetic Mg calcites display radically different behaviors from those of  
444 the end members as they diverge from both the calcite-dolomite and the calcite-magnesite  
445 lines (Fig. 8). The fitting curves are parabolas with maxima located between 25 and 35 mol%  
446  $\text{MgCO}_3$ . According to Bischoff et al. (1985), the random substitution of Ca and Mg would be  
447 accompanied by changes around the carbonate ion. The increase of FWHM as a function of  
448 magnesium content would be the result of increasing positional disorder of the carbonate ion  
449 and particularly of the rotation of these ions out of the basal plane, around the  $a$  axes. This  
450 disorder would prevail in the neighborhood of the Mg ions to accommodate shorter bonds.  
451 The hypothesis of carbonate positional disorder proposed by Bischoff et al. (1985) has been  
452 questioned by Falini et al. (1998), Zolotoyabko et al. (2010) and Wang et al. (2012).  
453 However, although the origin of Raman band enlargement due to the presence of magnesium  
454 is debated, there is a consensus on the fact that the random distribution of Mg in calcite  
455 increases the distribution of metal-O bond lengths in the crystal, which in turn increases the  
456 FWHM of the Raman bands (Wang et al., 2012). The idea that the number of metal-O  
457 configurations affects the FWHM of the Raman modes in synthetic calcites could explain the  
458 parabola shape of the FWHM as a function of composition. However, in case of random  
459 distribution, one would expect the maximum of different metal-O configurations to be located  
460 at  $\sim 50$  mol%  $\text{MgCO}_3$ . For instance, this is what is observed in the aragonite-strontianite solid  
461 solution (Alia et al., 1997), their Fig. 4b. On the other hand, if the distribution of atoms is not

462 random and some short range dolomite-type ordering (alternating layers of Ca and Mg)  
463 appears, one would expect the maximum of metal-O configurations to be located between  
464 calcite and dolomite, and not calcite and magnesite. This situation would translate into  
465 FWHM maxima between calcite and dolomite as observed in our experiments. Thus, these  
466 new data can be interpreted in terms of progressive ordering or clustering of Ca and Mg in  
467 cation layers, starting at about 10 mol% MgCO<sub>3</sub> and evolving towards a generalized  
468 dolomite-like ordering.

#### 469 **Comparison with magnesian amorphous calcium carbonate**

470 Wang et al. (2012) synthesized a series of ACC with magnesium contents in the range 0 to 43  
471 mol% MgCO<sub>3</sub>. According to Wang et al. (2012), two internal modes are observed in ACC:  
472 the symmetric and antisymmetric C-O stretches ( $\nu_1$  and  $\nu_3$ , respectively). The results obtained  
473 by Wang et al. (2012) on the  $\nu_1$  mode are displayed in Fig. 7d. Compared with Mg calcites,  
474 Mg-ACC  $\nu_1$  wavenumbers are systematically shifted towards lower wavenumbers; in  
475 addition, they increase as Mg increases along a slope similar to the one of Mg calcites, but  
476 with lower intercept and greater data dispersion. It should also be noted that the dispersion of  
477 data increases above 30 mol% MgCO<sub>3</sub> (Fig. 7d). The  $\nu_1$  FWHM of Mg-ACC are higher than  
478 those of the magnesian calcites (greater than 22 cm<sup>-1</sup>); they also depend on the Mg contents  
479 (Fig. 8d). The FWHM ACC data align along a straight line, while the  $\nu_1$  FWHM of the Mg  
480 calcites align along a curve up to 30 mol% MgCO<sub>3</sub> [Fig. 8d (see also the supplementary data  
481 Fig. EA2)]; the sudden change of slope of Mg calcites at about 27 mol% MgCO<sub>3</sub> has been  
482 discussed earlier and will not be reconsidered here].

483 Wang et al. (2012) explained the positional shift and the increase of the FWHM of the  
484 Mg-ACC  $\nu_1$  mode as a function of Mg content by differences between Ca-O and Mg-O bonds.  
485 Interestingly, in a similar way to what is observed for the Mg calcite  $\nu_1$  band (Fig. EA1), these  
486 authors observed that the Mg-ACC  $\nu_1$  peaks show some asymmetry that becomes more

487 pronounced as the peak broadens with increasing Mg contents above 30 mol % MgCO<sub>3</sub>. The  
488 ACC peak asymmetry could also be fit with two discrete peaks. According to these authors  
489 that  $\nu_1$  peak could be a convolution of two (or more) discrete peaks, potentially invalidating a  
490 solid solution model. It may suggest that high-Mg-ACC could correspond to a heterogeneous  
491 mixture of both calcium and magnesium amorphous carbonate, rather than as a solid solution  
492 (Wang et al., 2012). Note that the authors underlined the fact that this conclusion remained  
493 hypothetical and required further investigation. In all cases, the analogy related to peak  
494 doubling between amorphous and crystalline carbonates is striking. Concerning the  
495 differences between the spectral properties of Mg-ACC and Mg calcites, the systematic  
496 positional shift of the  $\nu_1$  mode toward lower wavenumbers and larger FWHM of Mg-ACC can  
497 be attributed to the fact that Mg-ACC are disordered solids, without order beyond 1.5 nm  
498 (Michel et al., 2008; Wang et al., 2012).

499  
500

### Implications

501 *Raman properties and Mg contents of abiotic and biogenic calcites* - In addition to providing  
502 structural information, the Raman properties of Ca-Mg carbonates allow assessing the Mg  
503 contents of inorganic calcites with a good degree of confidence. In principle, these results  
504 could also be applied to biogenic calcites. However, Bischoff et al. (1985) noted singular  
505 Raman properties of biogenic calcites with respect to their inorganic counterparts. Thus, it is  
506 probable that features specific to biominerals such as small grain size, structural order,  
507 occluded organic matter, substitution of trace elements, and variability of composition may  
508 affect Raman spectra of biogenic calcites. Further work is required to characterize and  
509 understand the origin of the Raman singularities of biogenic Mg calcites.

510 *Mg calcite versus Mg ACC* – Whether the results of Wang et al. (2012) on synthetic  
511 magnesian amorphous calcium carbonates can be applied to natural ACCs in biominerals is

512 not yet determined as interactions with organic molecules may play a role just as in the case  
513 of biogenic calcites. Considering the difference of spectral properties between synthetic Mg  
514 calcites and Mg-ACC, the determination of the crystalline or amorphous nature of an  
515 unknown carbonate is required prior to determining its Mg composition with Raman  
516 properties. Wavenumbers are not perfectly discriminant between Mg ACCs and Mg calcites  
517 because of potential overlap in the range 1086-1090  $\text{cm}^{-1}$ . On another hand, there is no  
518 overlap of FWHM between the two types of materials, which makes FWHM a good criterion  
519 to distinguish Mg ACCs from Mg calcites. Considering the range 0-30 mol%  $\text{MgCO}_3$   
520 particularly important for biominerals,  $\nu_1$  wavenumbers lower than 1086  $\text{cm}^{-1}$  and  $\nu_1$  FWHM  
521 greater than 22  $\text{cm}^{-1}$  are two adequate criteria to determine the amorphous nature of calcium  
522 carbonate in Raman spectra.

523 *The nature of dolomite-like ordering in Mg calcites* – As a general rule, intermediate  
524 compounds with superlattices may form in solid solutions if the radii of the involved cations  
525 differ by more than 15% (see Deelman (2003) for a review). In this respect, ordered dolomite  
526 is a superlattice of calcite or magnesite. Concerning the structural transition between calcite  
527 and ordered dolomite, we favor progressive dolomite like ordering rather than random  
528 substitution of Ca and Mg. This conclusion raises the question of the nature of this order. On  
529 the basis of enthalpy, entropy and volume data of Mg calcites synthesized in the range 0-12.4  
530 mol%  $\text{MgCO}_3$ , Navrotsky and Capobianco (1987) cautiously proposed a structure with Ca  
531 layers randomly interspersed with Mg-rich layers. For example, for a magnesian calcite  
532 containing 10 mol%  $\text{MgCO}_3$ , one layer in nine would be Mg-rich. These authors emphasized  
533 that such Mg-rich layers would occur at random in the stacking sequence and that the molar  
534 volumes would fall near the weighted average for calcite and dolomite. Instead of such a  
535 stacking of Ca or Mg layers, we prefer the idea of Mg clustering within a basal layer. This  
536 planar arrangement could be combined with ordering between successive basal planes so that

537 a 3D short-range dolomite-like order would appear. The frequency and size of these 3D short-  
538 range dolomite-like clusters would increase with Mg content. This model is proposed as a  
539 working hypothesis considering that it is not yet sustained by direct observation or numerical  
540 simulation. Whatever the model selected [stacking of Mg layers (Navrotsky and Capobianco,  
541 1987), or cation ordering in successive cation basal layers (the present work)], both studies  
542 converge to conclude that Mg calcites show significant local order. Despite repeated efforts to  
543 find specific dolomite reflections in diffractograms of Mg calcites, such reflections have never  
544 been observed below 42.5 mol% MgCO<sub>3</sub> (Goldsmith et al., 1961; Mackenzie et al., 1983).  
545 And yet, the band at 880 cm<sup>-1</sup> is observed in syntheses with Mg contents as low as ~10 mol%  
546 MgCO<sub>3</sub>. This could be ascribed to the fact that Raman spectroscopy is a more sensitive probe  
547 of local structural order than XRD which is known to probe the overall average long range  
548 order of crystalline materials (Doriguetto et al., 2004; Lekgoathi and Kock, 2016). If the range  
549 of order probed by Raman and XRD differ (e.g. <5 nm and >10 nm, respectively) the fact that  
550 dolomite-like order is detected by Raman and not by powder XRD could provide an upper  
551 limit for the size of the dolomite-like clusters (i.e. less than 10 nm if the above numbers are  
552 accepted). It is often considered that physical and spectroscopic properties of carbonates vary  
553 linearly with cation radius or mass (Railsback, 1999). The fact that it is not the case for the  
554 Raman properties of Mg calcites can be tentatively ascribed to the contribution of structural  
555 order to the Raman spectral properties of these carbonates.

## 556 **Acknowledgments**

557

558 This work has been supported by the Centre National de la Recherche Scientifique (CNRS),  
559 by Institut National des Sciences de l'Univers (INSU) through grant INTERRVIE 2013, by  
560 the Agence National pour la Recherche (ANR) through ANR CoRo 2011-2015, by the Centre  
561 Interdisciplinaire de Nanosciences de Marseille (CINaM), and by the European Union COST

562 action TD0903. This work has been partly carried out within the framework of the ICoME2  
563 Labex (ANR-11-LABX-0053) and the A\*MIDEX projects (ANR-11-IDEX-0001-02)  
564 cofunded by the French programme 'Investissements d'Avenir', which is managed by the  
565 ANR, the French National Research Agency. Observations were made on a FESEM financed  
566 by the European Fund for Regional Development (EFRD). We thank F. Bedu and I. Ozerov  
567 for their assistance on this instrument and B. Devouard for providing the OCN calcite. We  
568 thank J. L. Devidal and N. Bolfan-Casanova (LMV, Clermond-Fd) for his assistance with  
569 electron microprobe and  $\mu$ -Raman, respectively. D.V. benefited from a financial support by  
570 E.M. Stolper for a three month stay at Caltech in 2014, where and when most of the  $\mu$ -Raman  
571 analyses were made. Reviews by R.L. Frost and an anonymous reviewer as well as editorial  
572 handling by R. Stalder are gratefully acknowledged. This is contribution ANR CoRo n° 09.  
573

574

## Bibliography

- 575 Addadi, L., Raz, S., and Weiner, S. (2003) Taking advantage of disorder: Amorphous calcium  
576 carbonate and its roles in biomineralization. *Advanced Materials*, 15(12), 959-970.  
577 Alia, J.M., de Mera, Y.D., Edwards, H.G.M., Martin, P.G., and Andres, S.L. (1997) FT-  
578 Raman and infrared spectroscopic study of aragonite-strontianite ( $\text{Ca}_x\text{Sr}_{1-x}\text{CO}_3$ ) solid  
579 solution. *Spectrochimica Acta Part a-Molecular and Biomolecular Spectroscopy*,  
580 53(13), 2347-2362.  
581 Bathurst, R. (1975) *Carbonate Sediments and Their Diagenesis*. Elsevier, Amsterdam.  
582 Beniash, E., Aizenberg, J., Addadi, L., and Weiner, S. (1997) Amorphous calcium carbonate  
583 transforms into calcite during sea urchin larval spicule growth. *Proceedings of the*  
584 *Royal Society B-Biological Sciences*, 264(1380), 461-465.  
585 Benzerara, K., Menguy, N., Lopez-Garcia, P., Yoon, T.H., Kazmierczak, J., Tyliszczak, T.,  
586 Guyot, F., and Brown, G.E. (2006) Nanoscale detection of organic signatures in  
587 carbonate microbialites. *Proceedings of the National Academy of Sciences of the*  
588 *United States of America*, 103(25), 9440-9445.  
589 Bhagavantam, S., and Venkatarayudu, T. (1939) Raman effect in relation to crystal structure.  
590 *Proceedings of the Indian Academy of Sciences, Section A*, 9, p. 224-258. Indian  
591 Academy of Sciences.  
592 Bischoff, W.D., Bishop, F.C., and Mackenzie, F.T. (1983) Biogenically produced magnesian  
593 calcite inhomogeneities in chemical and physical-properties comparison with synthetic  
594 phases. *American Mineralogist*, 68(11-1), 1183-1188.  
595 Bischoff, W.D., Sharma, S.K., and Mackenzie, F.T. (1985) Carbonate ion disorder in  
596 synthetic and biogenic magnesian calcites - A Raman spectral study. *American*  
597 *Mineralogist*, 70(5-6), 581-589.  
598 Boulard, E., Menguy, N., Auzende, A., Benzerara, K., Bureau, H., Antonangeli, D., Corgne,  
599 A., Morard, G., Siebert, J., and Perrillat, J.-P. (2012) Experimental investigation of the  
600 stability of Fe-rich carbonates in the lower mantle. *Journal of Geophysical Research:*  
601 *Solid Earth* (1978–2012), 117(B2).  
602 Byrnes, A.P., and Wyllie, P.J. (1981) Subsolidus and melting relations for the join  $\text{CaCO}_3$ -  
603  $\text{MgCO}_3$  at 10 kbar. *Geochimica Et Cosmochimica Acta*, 45(3), 321-328.  
604 Cabannes, J., and Aynard, R. (1942) Étude expérimentale et théorique sur le spectre Raman  
605 de l'eau de cristallisation dans le gypse. *J. Phys. radium*, 3(8), 137-145.  
606 Chave, K.E. (1954a) Aspects of the biogeochemistry of magnesium 1. Calcareous marine  
607 organisms. *The Journal of Geology*, 266-283.  
608 -. (1954b) Aspects of the biogeochemistry of magnesium 2. Calcareous sediments and rocks.  
609 *The Journal of Geology*, 587-599.  
610 Couture, L. (1947) Etude des spectres de vibration de monocristaux ioniques. *Annales de*  
611 *physique*, 2, p. 5-94. EDP Sciences.  
612 Deelman, J. (2003) Low-temperature formation of dolomite and magnesite. Compact disc  
613 publications v2.3.  
614 Doriguetto, A.C., Boschi, T.M., Pizani, P.S., Mascarenhas, Y.P., and Ellena, J. (2004) The  
615 effect of the cation substitution on the structural and vibrational properties of  
616  $\text{Cs}_2\text{NaGaxSc}_{1-x}\text{F}_6$  solid solution. *Journal of Chemical Physics*, 121(7), 3184-3190.  
617 Dresselhaus, M., Dresselhaus, G., and Hofmann, M. (2008) Raman spectroscopy as a probe of  
618 graphene and carbon nanotubes. *Philosophical Transactions of the Royal Society of*  
619 *London A: Mathematical, Physical and Engineering Sciences*, 366(1863), 231-236.  
620 Falini, G., Fermani, S., Gazzano, M., and Ripamonti, A. (1998) Structure and morphology of  
621 synthetic magnesium calcite. *Journal of Materials Chemistry*, 8(4), 1061-1065.  
622 Finch, A.A., and Allison, N. (2007) Coordination of Sr and Mg in calcite and aragonite.  
623 *Mineralogical Magazine*, 71(5), 539-552.



- 624 Goldsmith, J., Graf, D., and Heard, H. (1961) Lattice constants of the calcium-magnesium  
625 carbonates, 46, p. 453-457. Mineralogical Soc Amer 1015 Eighteenth St, NW Suite  
626 601, Washington, DC 20036.
- 627 Goldsmith, J.R., and Heard, H.C. (1961) Subsolidus phase relations in the system. The  
628 Journal of Geology, 45-74.
- 629 Irving, A.J., and Wyllie, P.J. (1975) Subsolidus and melting relationships for calcite,  
630 magnesite and the join  $\text{CaCO}_3\text{-MgCO}_3$  36 kb. *Geochimica Et Cosmochimica Acta*,  
631 39(1), 35-53.
- 632 Kastler, A., and Rousset, A. (1941) L'effet Raman et le pivotement des molécules dans les  
633 cristaux. Théorie générale et vérification expérimentale dans le cas du naphthalène. *J.*  
634 *phys. radium*, 2(2), 49-57.
- 635 Krishnamurti, D. (1956) Raman spectrum of magnesite. *Proceedings of the Indian Academy*  
636 *of Sciences-Section A*, 43, p. 210-212. Springer.
- 637 Krishnan, R. (1945) Raman spectra of the second order in crystals Part I: Calcite. *Proceedings*  
638 *of the Indian Academy of Sciences, Section A*, 22, p. 182-193. Indian Academy of  
639 Sciences.
- 640 Land, L.S. (1967) Diagenesis of skeletal carbonates. *Journal of Sedimentary Petrology*, 37,  
641 914-930.
- 642 Lekgoathi, M.D.S., and Kock, L.D. (2016) Effect of short and long range order on crystal  
643 structure interpretation: Raman and powder X-ray diffraction of  $\text{LiPF}_6$ .  
644 *Spectrochimica Acta Part A: Molecular and Biomolecular Spectroscopy*, 153, 651-  
645 654.
- 646 Long, X., Nasse, M.J., Ma, Y., and Qi, L. (2012) From synthetic to biogenic Mg-containing  
647 calcites: a comparative study using FTIR microspectroscopy. *Physical Chemistry*  
648 *Chemical Physics*, 14(7), 2255-2263.
- 649 Mackenzie, F.T., Bischoff, W.D., Bishop, F.C., Loijens, M., Schoonmaker, J., and Wollast, R.  
650 (1983) Magnesian calcites; low-temperature occurrence, solubility and solid-solution  
651 behavior. *Reviews in Mineralogy and Geochemistry*, 11(1), 97-144.
- 652 Michel, F.M., MacDonald, J., Feng, J., Phillips, B.L., Ehm, L., Tarabrella, C., Parise, J.B.,  
653 and Reeder, R.J. (2008) Structural characteristics of synthetic amorphous calcium  
654 carbonate. *Chemistry of Materials*, 20(14), 4720-4728.
- 655 Morse, J.W., Arvidson, R.S., and Lüttge, A. (2007) Calcium carbonate formation and  
656 dissolution. *Chemical Reviews*, 107(2), 342-381.
- 657 Navrotsky, A., and Capobianco, C. (1987) Enthalpies of formation of Dolomite and  
658 magnesian calcites. *American Mineralogist*, 72(7-8), 782-787.
- 659 Politi, Y., Arad, T., Klein, E., Weiner, S., and Addadi, L. (2004) Sea urchin spine calcite  
660 forms via a transient amorphous calcium carbonate phase. *Science*, 306(5699), 1161-  
661 1164.
- 662 Politi, Y., Batchelor, D.R., Zaslansky, P., Chmelka, B.F., Weaver, J.C., Sagi, I., Weiner, S.,  
663 and Addadi, L. (2010) Role of Magnesium Ion in the Stabilization of Biogenic  
664 Amorphous Calcium Carbonate: A Structure-Function Investigation. *Chemistry of*  
665 *Materials*, 22(1), 161-166.
- 666 Politi, Y., Levi-Kalishman, Y., Raz, S., Wilt, F., Addadi, L., Weiner, S., and Sagi, I. (2006)  
667 Structural characterization of the transient amorphous calcium carbonate precursor  
668 phase in sea urchin embryos. *Advanced Functional Materials*, 16(10), 1289-1298.
- 669 Railsback, L.B. (1999) Patterns in the compositions, properties, and geochemistry of  
670 carbonate minerals. *Carbonates and Evaporites*, 14(1), 1-20.
- 671 Roisnel, T., and Rodríguez-Carvajal, J. (2001) WinPLOTR: a windows tool for powder  
672 diffraction pattern analysis. *Materials Science Forum*, 378, p. 118-123. Transtec  
673 Publications; 1999.

- 674 Rutt, H., and Nicola, J. (1974) Raman spectra of carbonates of calcite structure. *Journal of*  
675 *Physics C: Solid State Physics*, 7(24), 4522.
- 676 Schauble, E.A., Ghosh, P., and Eiler, J.M. (2006) Preferential formation of C-13-O-18 bonds  
677 in carbonate minerals, estimated using first-principles lattice dynamics. *Geochimica Et*  
678 *Cosmochimica Acta*, 70(10), 2510-2529.
- 679 Tao, J.H., Zhou, D.M., Zhang, Z.S., Xu, X.R., and Tang, R.K. (2009) Magnesium-aspartate-  
680 based crystallization switch inspired from shell molt of crustacean. *Proceedings of the*  
681 *National Academy of Sciences of the United States of America*, 106(52), 22096-  
682 22101.
- 683 Valenzano, L., Noel, Y., Orlando, R., Zicovich-Wilson, C.M., Ferrero, M., and Dovesi, R.  
684 (2007) Ab initio vibrational spectra and dielectric properties of carbonates: magnesite,  
685 calcite and dolomite. *Theoretical Chemistry Accounts*, 117(5-6), 991-1000.
- 686 Vielzeuf, D., Baronnet, A., Perchuk, A.L., Laporte, D., and Baker, M.B. (2007) Calcium  
687 diffusivity in alumino-silicate garnets: an experimental and ATEM study.  
688 *Contributions to Mineralogy and Petrology*, 154(2), 153-170.
- 689 Wang, D.B., Hamm, L.M., Bodnar, R.J., and Dove, P.M. (2012) Raman spectroscopic  
690 characterization of the magnesium content in amorphous calcium carbonates. *Journal*  
691 *of Raman Spectroscopy*, 43(4), 543-548.
- 692 Wang, D.B., Wallace, A.F., De Yoreo, J.J., and Dove, P.M. (2009) Carboxylated molecules  
693 regulate magnesium content of amorphous calcium carbonates during calcification.  
694 *Proceedings of the National Academy of Sciences of the United States of America*,  
695 106(51), 21511-21516.
- 696 Weiner, S., Sagi, I., and Addadi, L. (2005) Choosing the crystallization path less traveled.  
697 *Science*, 309(5737), 1027-1028.
- 698 Weiss, I.M., Tuross, N., Addadi, L., and Weiner, S. (2002) Mollusc larval shell formation:  
699 Amorphous calcium carbonate is a precursor phase for aragonite. *Journal of*  
700 *Experimental Zoology*, 293(5), 478-491.
- 701 White, W.B. (1974a) The carbonate minerals. In E. V. C. Farmer, Ed. *The Infra-red Spectra*  
702 *of Minerals*, Mineralogical Society Monograph 4, p. 227-284. Mineralogical Society,  
703 London.
- 704 -. (1974b) Order-disorder effects. In E. V. C. Farmer, Ed. *The Infra-red Spectra of*  
705 *Minerals*, Mineralogical Society Monograph 4 p. 87-110. Mineralogical Society,  
706 London.
- 707 Zolotoyabko, E., Caspi, E.N., Fieramosca, J.S., Von Dreele, R.B., Marin, F., Mor, G., Addadi,  
708 L., Weiner, S., and Politi, Y. (2010) Differences between Bond Lengths in Biogenic  
709 and Geological Calcite. *Crystal Growth & Design*, 10(3), 1207-1214.

710

711

712

713

### Figure captions:

714 **Figure 1:** Raman spectra of calcite, dolomite and magnesite optically clear natural (OCN)  
715 crystals. (a-b) T and L lattice modes, (c-f)  $\nu_4$ ,  $\nu_1$ ,  $\nu_3$  and  $2\nu_2$  internal modes.

716

717 **Figure 2:** SEM-BSE images of synthetic magnesian calcites showing 100 to 200  $\mu\text{m}$   
718 polyhedral crystals. Homogeneous grey level in a given grain indicates homogeneous crystal  
719 composition; variation of grey level from one grain to another result from variations of lattice  
720 orientations. Note the presence of pores between the crystals.

721

722 **Figure 3:** Compositions (mol%  $\text{MgCO}_3$ ) of the synthetic Mg calcites determined by electron  
723 microprobe plotted against nominal compositions. (Error bars are smaller than symbols).

724

725 **Figure 4:** Raman spectra of some synthetic magnesian calcites. (a-b) T and L lattice modes;  
726 (c-f)  $\nu_4$ ,  $\nu_1$ ,  $\nu_3$  and  $2\nu_2$  internal modes. The spectra of OCN calcite, dolomite and magnesite are  
727 reported for comparison. Abbreviations: Cal: calcite; Dol: dolomite; Mgs: magnesite. Laser  
728 514.5 nm, accumulation of 5 scans.

729

730 **Figure 5:** Wavenumber of the different Raman modes of synthetic Mg calcites as a function of  
731 composition in the range 0-30 mol%  $\text{MgCO}_3$ . The straight lines joining the calcite spectral  
732 data to the dolomite data (Cal-Dol) or to the magnesite data (Cal-Mgs) are shown for  
733 comparison. Fitting parameters of the 3<sup>rd</sup> order polynomials are given in [Table 3](#) (valid  
734 within the range 0-30 mol%  $\text{MgCO}_3$ ).

735

736 **Figure 6:** Full width at half maximum (FWHM) of the Raman modes of synthetic Mg calcites  
737 as a function of composition in the range 0-30 mol% MgCO<sub>3</sub>. The Cal-Dol and Cal-Mgs lines  
738 (dashed and dash-dotted lines, respectively) are shown for comparison. The fitting  
739 parameters of the 2<sup>nd</sup> order polynomials are given in [Table 3](#).

740

741 **Figure 7:** Wavenumber of the Raman modes of synthetic Mg calcites as a function of  
742 composition in the range 0-50 mol% MgCO<sub>3</sub>. The red squares are from Bischoff et al.,  
743 (1985). Blue squares in [Fig. 7d](#) correspond to magnesian amorphous calcium carbonates  
744 from Wang et al., (2012). The Cal-Dol (green) and Cal-Mgs lines (blue) are also shown. The  
745 fitting parameters of the linear equations are listed in [Table 4](#).

746

747 **Figure 8:** Full width at half maximum of the Raman modes of synthetic Mg calcites as a  
748 function of composition in the range 0-50 mol% MgCO<sub>3</sub>. The red squares are from Bischoff et  
749 al., (1985). Blue squares in [Fig. 8d](#) correspond to magnesian amorphous calcium carbonates  
750 from Wang et al., (2012). The Cal-Dol (green) and Cal-Mgs lines (blue) are also shown. The  
751 fitting parameters of the linear equations are listed in [Table 4](#).

752

753 **Figure 9:** Raman spectra of calcite, dolomite and magnesite gem crystals, and synthetic Mg  
754 calcites in the range 840-920 cm<sup>-1</sup>. Spectra were normalized to the  $\nu_1$  intensity; baselines  
755 were extracted following a similar process for all spectra. A second series of measurements  
756 with improved signal/noise ratio is shown in the inset. It indicates that the  $\nu_2$  peak could  
757 appear as soon as ~10 mol% MgCO<sub>3</sub>. In the inset, spectra were normalized to the  $\nu_4$  intensity.

758

759 **Figure EA-1:** Simple (a, c) and double (b, d) peak fitting for Mg calcite syntheses with 14.5  
760 and 37.8 mol% MgCO<sub>3</sub>.

761

762 **Figure EA-2:** (a) Wavenumber of the  $\nu_1$  Raman mode of synthetic Mg calcites as a function of  
763 composition in the range 0-50 mol% MgCO<sub>3</sub>. Results of simple and double peak fittings are  
764 shown in red and black, respectively. Cal-Dol and Cal-Mgs lines are shown for comparison.  
765 (b) FWHM of the  $\nu_1$  Raman mode of synthetic Mg calcites as a function of composition in the  
766 range 0-30 and 0-50 mol% MgCO<sub>3</sub> for the simple (red) and double (black) peak fitting,  
767 respectively.

768

769

## Supplementary materials:

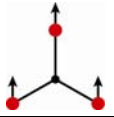
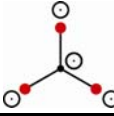
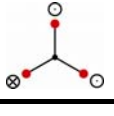
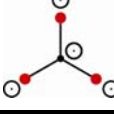
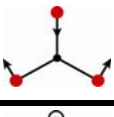
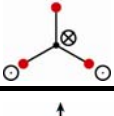
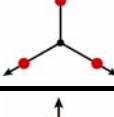
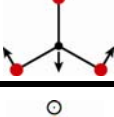
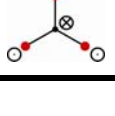
770 EA1 –  $\nu_1$  Peak doubling

771 **Figure EA1** shows the  $\nu_1$  mode of Mg calcites containing 14.5 and 37.8 mol%  $\text{MgCO}_3$ .  
772 The peak becomes asymmetric to the left as Mg increases, and increasingly difficult to fit  
773 with a single peak. This simple fact explains the features observed in **Fig. 8d** with a marked  
774 change of trend above 30 mol%  $\text{MgCO}_3$ . The one- and two-peak fits are shown in **Fig. EA1**.  
775 For the two-peak fit, the constraint of FWHM similarity for the two peaks had to be  
776 introduced to minimize the number of potential solutions. **Figure EA2a** shows the peak  
777 wavenumbers as a function of Mg content. The position of the major peak is close to that  
778 determined with a single peak. The position of the second peak departs significantly from the  
779 one of the first peak, with higher data dispersion. However, the slopes of the two datasets are  
780 similar. As far as FWHM is concerned (**Fig. EA2b**), the data alignment is better than in the  
781 one-peak fit and does no longer show divergence at 30 mol%  $\text{MgCO}_3$ . As in the case of  $2\nu_2$ , a  
782 maximum seems to be reached at about 50 mol%  $\text{MgCO}_3$ . However, this conclusion is  
783 difficult to ascertain as no data were collected above 50 mol%  $\text{MgCO}_3$ . Note that for the  
784 double peak fitting, a single set of FWHM is reported on this figure as the constraint of  
785 similarity of FWHM for the two peaks was introduced in the model.

786 The main purpose of these supplementary materials is to explain the particular  
787 behavior of the  $\nu_1$  FWHM above  $\sim 30$  mol%  $\text{MgCO}_3$  (**Fig. 8d**). They indicate that the Raman  
788 spectra of the Ca-Mg carbonate solid-solution may show more complicated features than  
789 expected. The origin of peak doubling as Mg increases in the solid-solution is not yet fully  
790 understood, though a tentative explanation is provided in the main text.

791

**Table 1:** Raman modes for Ca-Mg carbonates. Wavenumber ranges come from the present study. For complete reviews of carbonate modes see Schauble et al. (2006), Valenzano et al. (2007) and Gillet et al. (1993).

Main notation	Space group notation	Schematic of vibration	Type of vibration	Geometry of vibration	Wavenumber range (cm <sup>-1</sup> )	Comments	Vibration type attribution
T	(E <sub>g</sub> )		External	In Plane Translation	155-212	Doubly degenerate	(Kastler and Rousset, 1941), (Cabannes and Aynard, 1942), (Couture, 1947)
235 cm <sup>-1</sup>	(A <sub>g</sub> )		External	Vertical Translation	230-240	Only active in dolomite	(Valenzano et al., 2007)
L	(E <sub>g</sub> )		External	Libration	282-331	Doubly degenerate	(Kastler and Rousset, 1941), (Cabannes and Aynard, 1942)
335 cm <sup>-1</sup>	(A <sub>g</sub> )		External	Vertical Translation	330-340	Only active in dolomite	(A <sub>2g</sub> ) mode in magnesite (Valenzano et al., 2007)
ν <sub>4</sub>	(E <sub>g</sub> )		Internal	In Plane Bending	711-740	Doubly degenerate	(Kastler and Rousset, 1941), (Cabannes and Aynard, 1942), (Couture, 1947)
ν <sub>2</sub>	(A <sub>g</sub> )		Internal	Out of Plane Bending	872-881	Only active in dolomite	(A <sub>2g</sub> ) mode in calcite and magnesite (Schauble et al., 2006)
ν <sub>1</sub>	(A <sub>1g</sub> )		Internal	Symmetric Stretch	1086-1095	Active as (A <sub>g</sub> ) mode in dolomite	(Kastler and Rousset, 1941), (Cabannes and Aynard, 1942), (Couture, 1947)
ν <sub>3</sub>	(E <sub>g</sub> )		Internal	Anti-Symmetric Stretch	1435-1446	Doubly degenerate	(Kastler and Rousset, 1941), (Cabannes and Aynard, 1942), (Couture, 1947)
2 ν <sub>2</sub>	(A <sub>2g</sub> )		Internal	Out of Plane Bending	1748-1763	Overtone of the silent ν <sub>2</sub> mode in most Ca-Mg carbonate	(Kastler and Rousset, 1941), (Cabannes and Aynard, 1942), (Couture, 1947)

- 1 **Table 2:** *Wavenumbers and FWHM (in italics) of all Raman modes of calcite, dolomite and magnesite OCN crystals and other reference crystals*
- 2 *from the literature (units in  $\text{cm}^{-1}$ ).*



External (or lattice) modes					Internal modes				
	T	230 cm <sup>-1</sup>	L	340 cm <sup>-1</sup>	$\nu_4$	$\nu_2$	$\nu_1$	$\nu_3$	$2\nu_2$
<b>Calcite</b> OCN crystal	155.5 6.5	Inactive	282 9.7	Inactive	711.8 3.1	Inactive	1086 3.1	1435.6 4.7	1748.7 7.5
<b>Calcite</b> (Bischoff et al., 1985)	154 6.2	Inactive	281 10.1	Inactive	711 3.6	Inactive	1085 2.5	1434 2.0	1748 3.6
<b>Calcite</b> (theoretical) (Schauble et al., 2006)	155.5	Inactive	273	310.4 (A <sub>2g</sub> )	711	872.5 (A <sub>2g</sub> )	1094.3	1437.6	∅
<b>Dolomite</b> Azcarate OCN crystal	177.1 6.1		301.1 9.3	340	723.9 9.3	881	1098.1 6	1442.5 7.2	1757.7 10.4
<b>Dolomite</b> (Bischoff et al., 1985)	175 5.5		299 9.8	335	724 9.0	Not observed	1097 6.1	1441 3.8	1756 4.3
<b>Dolomite</b> (theoretical) (Schauble et al., 2006)	176.2	231.2	295.8	338.3 (A <sub>g</sub> )	724.7	876.5	1104.4	1446.6	∅
<b>Magnesite</b> Brumado OCN crystal	213.6 3.7	Inactive	331 4.4	Inactive	738.1 15.8	Inactive	1094.9 13.2	1445.8 6.7	1763 10.1
<b>Magnesite</b> (Bischoff et al., 1985)	213 4.0	Inactive	329 4.9	Inactive	738 12.2	Inactive	1093 12.5	1444 3.1	1762 4.8
<b>Magnesite</b> (theoretical) (Schauble et al., 2006)	208.4	Inactive	324.4	361.7 (A <sub>2g</sub> )	737.7	875.9 (A <sub>2g</sub> )	1103.3	1452.6	∅

**Table 3:** Wavenumbers and FWHM (in italics) of the six Raman modes of synthetic Mg calcites (units in  $\text{cm}^{-1}$ ). Experiments were named after the nominal composition of the starting material; the composition measured with the electron microprobe is given below each name (e.g. MgCc\_8 stands for a starting material with 8 mol%  $\text{MgCO}_3$  – the measured composition is 6.1 mol%  $\text{MgCO}_3$ ). Experiments MgCc\_2 to MgCc\_30 were carried out at 1 GPa, 1000°C, others at 1.5 GPa and 1100°C.

	T	L	$\nu_4$	$\nu_1$	$\nu_3$	$2 \nu_2$
MgCc_2	155.55	281.71	711.78	1086.34	1435.7	1749
0.7 mol% $\text{MgCO}_3$	<i>7.87</i>	<i>10.92</i>	<i>3.60</i>	<i>3.62</i>	<i>6.7</i>	<i>7.9</i>
MgCc_4	156.43	282.46	712.28	1086.94	1436.3	1749.3
3.2 mol% $\text{MgCO}_3$	<i>10.20</i>	<i>13.18</i>	<i>5.17</i>	<i>4.53</i>	<i>7.4</i>	<i>8.8</i>
MgCc_6	156.72	282.99	712.8	1087.00	1436.8	1749.6
4 mol% $\text{MgCO}_3$	<i>11.11</i>	<i>14.18</i>	<i>5.75</i>	<i>6.07</i>	<i>9.5</i>	<i>9.6</i>
MgCc_8	157.53	283.87	713.11	1087.5	1437	1749.8
6.1 mol% $\text{MgCO}_3$	<i>12.81</i>	<i>15.81</i>	<i>7.43</i>	<i>6.90</i>	<i>13.1</i>	<i>9.7</i>
MgCc_10	158.65	284.92	713.82	1088.2	1436.9	1750.1
9.7 mol% $\text{MgCO}_3$	<i>16.47</i>	<i>17.53</i>	<i>11.26</i>	<i>8.06</i>	<i>22.8</i>	<i>11</i>
MgCc_12	158.61	284.70	713.84	1088.06	1437.5	1750
9.5 mol% $\text{MgCO}_3$	<i>16.00</i>	<i>18.39</i>	<i>10.77</i>	<i>8.03</i>	<i>18.9</i>	<i>11</i>
MgCc_14	159.23	285.54	714.42	1088.78	1437.6	1750.4
11.6 mol% $\text{MgCO}_3$	<i>12.5</i>	<i>19.10</i>	<i>12.13</i>	<i>8.75</i>	<i>28.3</i>	<i>11.2</i>
MgCc_16	159.43	286.01	714.52	1088.78	1437.2	1750.6
12.5 mol% $\text{MgCO}_3$	<i>16.98</i>	<i>19.20</i>	<i>12.46</i>	<i>8.72</i>	<i>22.7</i>	<i>11.2</i>
MgCc_18	160.10	286.73	714.58	1089.01	1437.2	1750.4
14.5 mol% $\text{MgCO}_3$	<i>17.64</i>	<i>19.95</i>	<i>14.22</i>	<i>9.41</i>	<i>29</i>	<i>12</i>
MgCc_20	161.18	287.37	715.09	1089.6	1435.7	1750.9
16.3 mol% $\text{MgCO}_3$	<i>22.03</i>	<i>20.85</i>	<i>14.98</i>	<i>9.67</i>	<i>31.2</i>	<i>12.1</i>
MgCc_22	161.39	288.27	715.82	1089.97	1436	1751.3
18.2 mol% $\text{MgCO}_3$	<i>19.31</i>	<i>20.96</i>	<i>15.05</i>	<i>9.99</i>	<i>34.8</i>	<i>13.5</i>
MgCc_24	162.75	289.17	715.84	1090.49	1435.9	1751.6
20.7 mol% $\text{MgCO}_3$	<i>20.00</i>	<i>22.13</i>	<i>16.39</i>	<i>10.36</i>	<i>36.3</i>	<i>13.1</i>
MgCc_26	163.10	290.75	716.37	1090.86	1435.9	1752
22 mol% $\text{MgCO}_3$	<i>20.68</i>	<i>23.00</i>	<i>17.01</i>	<i>10.76</i>	<i>35.4</i>	<i>17</i>
MgCc_28	164.56	292.02	717.37	1091.36	1437.6	1752.6
24 mol% $\text{MgCO}_3$	<i>21.51</i>	<i>23.44</i>	<i>17.60</i>	<i>12.01</i>	<i>38.6</i>	<i>13.5</i>
MgCc_30	165.03	292.44	717.72	1091.85	1439	1752.7
25.7 mol% $\text{MgCO}_3$	<i>19.36</i>	<i>23.01</i>	<i>18.70</i>	<i>11.90</i>	<i>41.8</i>	<i>13.5</i>
MgCc_35-1*	167.03	291.56	718.49	1094.19	1437.49	1754.23
28.3 mol% $\text{MgCO}_3$	<i>16.33</i>	<i>22.39</i>	<i>18.18</i>	<i>15.77</i>	<i>48.69</i>	<i>13.01</i>
MgCc_35-2*	169.19	293.83	719.79	1095.28	1439.6	1754.98
33.3 mol% $\text{MgCO}_3$	<i>16.22</i>	<i>22.83</i>	<i>18.76</i>	<i>19.96</i>	<i>61.38</i>	<i>14.64</i>
MgCc_40	170.57	298.22	720.78	1094.47	1438.4	1755.1
37.8 mol% $\text{MgCO}_3$	<i>16.88</i>	<i>23.51</i>	<i>17.95</i>	<i>13.13</i>	<i>36.4</i>	<i>17.7</i>
MgCc_45	172.51	297.68	722.26	1096.59	1439.89	1756.83
41.4 mol% $\text{MgCO}_3$	<i>14.23</i>	<i>21.83</i>	<i>19.00</i>	<i>24.52</i>	<i>28.77</i>	<i>15.46</i>
MgCc_50	175.41	300.89	724.02	1098.78	1441	1758.21
49.2 mol% $\text{MgCO}_3$	<i>10.54</i>	<i>19.10</i>	<i>16.24</i>	<i>23.96</i>	<i>20.72</i>	<i>14.81</i>

\*A single experiment with two compositions

**Table 4:** Equation coefficients to estimate the magnesium content (mol% MgCO<sub>3</sub>) of inorganic calcites from their Raman wavenumbers and FWHM in the range 0-30 mol% MgCO<sub>3</sub> (cf. Figs 5 and 6). Parameter X is either the wavenumber or the FWHM of the T, L,  $\nu_4$ ,  $\nu_1$ ,  $\nu_3$  and  $2\nu_2$  modes (in cm<sup>-1</sup>).

	<b>T</b>	<b>L</b>	$\nu_4$	$\nu_1$	$\nu_3$	<b>2<math>\nu_2</math></b>
mol% MgCO <sub>3</sub> f[Wavenumber]	155.28+0.39 X -0.0078 X <sup>2</sup> +0.000293 X <sup>3</sup>	281.44+0.4 X -0.00743 X <sup>2</sup> +0.000359 X <sup>3</sup>	711.48+0.35 X -0.014 X <sup>2</sup> +0.000391 X <sup>3</sup>	1086.2+0.22 X -0.00276 X <sup>2</sup> +0.000106 X <sup>3</sup>	-	1748.93+0.15 X -0.00531 X <sup>2</sup> +0.000204 X <sup>3</sup>
R <sup>2</sup>	0.997	0.995	0.991	0.999	-	0.98
mol% MgCO <sub>3</sub> f[FWHM]	6.76+1.19 X -0.0287 X <sup>2</sup>	10.66+0.89 X -0.0156 X <sup>2</sup>	2.45+0.99 X -0.0147 X <sup>2</sup>	3.61+0.51 X -0.00787 X <sup>2</sup>	2.56+2.16 X -0.026 X <sup>2</sup>	7.67+0.38 X -0.00448 X <sup>2</sup>
R <sup>2</sup>	0.950	0.990	0.993	0.973	0.972	0.826

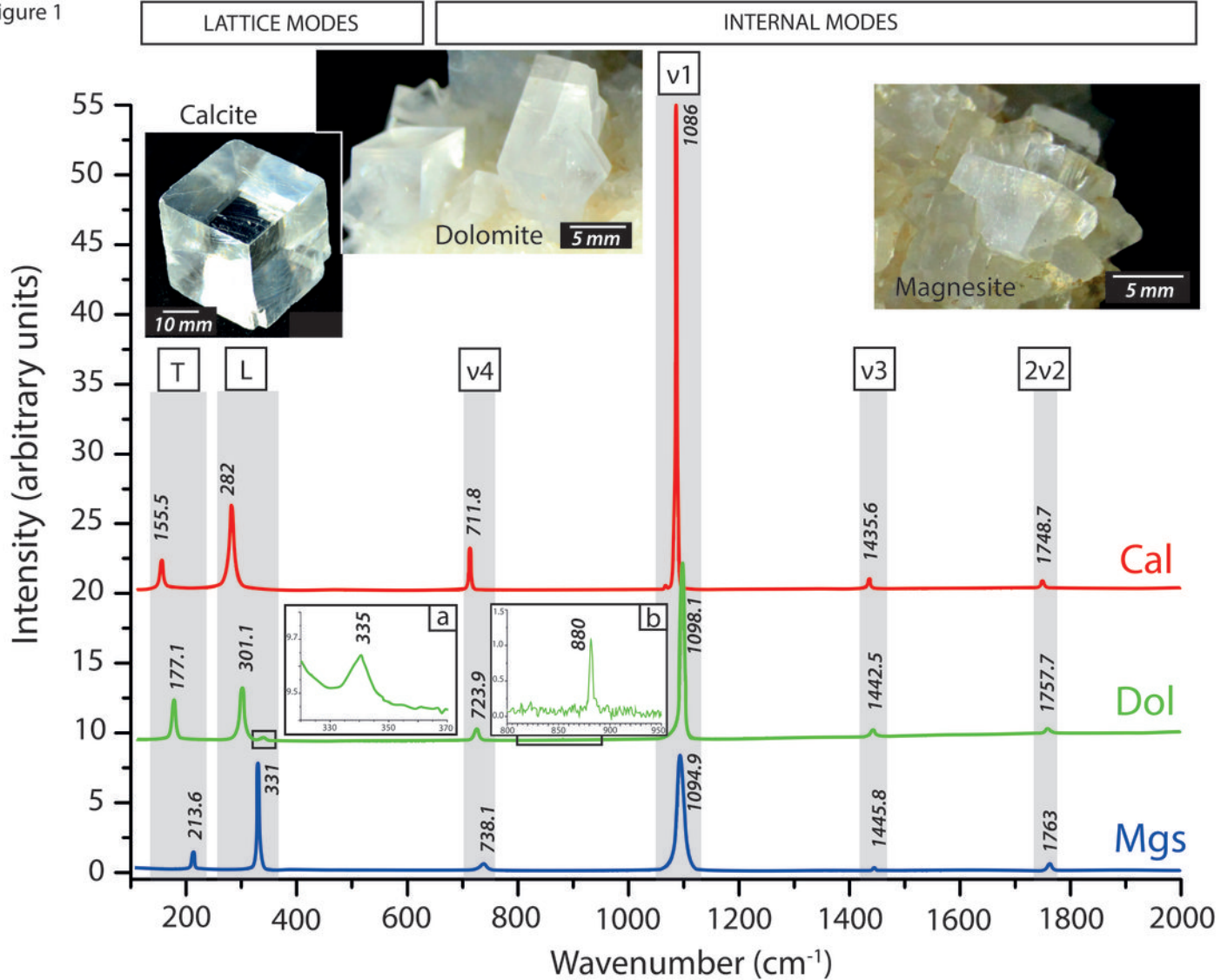
*Valid in the range 0-30 mol% MgCO<sub>3</sub>*

**Table 5:** Equation coefficients to estimate the magnesium content (mol% MgCO<sub>3</sub>) of inorganic calcites from their Raman wavenumbers (WN) and FWHM in the range 0-50 mol% MgCO<sub>3</sub> (see Fig. 7 and 8). Parameter X is either the wavenumber or the FWHM of the T, L,  $\nu_4$ ,  $\nu_1$ ,  $\nu_3$  and  $2\nu_2$  modes (in cm<sup>-1</sup>).

	T	L	$\nu_4$	$\nu_1$	$\nu_3$	$2\nu_2$
mol% MgCO <sub>3</sub> f[Wavenumber]	154.61 +0.418 X	281.16 +0.406 X	711.36 +0.25 X	1085.71 +0.256 X	-	1748.27 +0.191 X
R <sup>2</sup>	0.996	0.993	0.996	0.988	-	0.985
mol% MgCO <sub>3</sub> f[FWHM]	8.23+0.923 X -0.0183 X <sup>2</sup>	11.07+0.806 X -0.013 X <sup>2</sup>	2.7+0.952 X -0.0138 X <sup>2</sup>	-	1.78+2.98 X -0.05 X <sup>2</sup>	7.69+0.376 X -0.00448 X <sup>2</sup>
R <sup>2</sup>	0.950	0.983	0.990	-	0.84	0.836

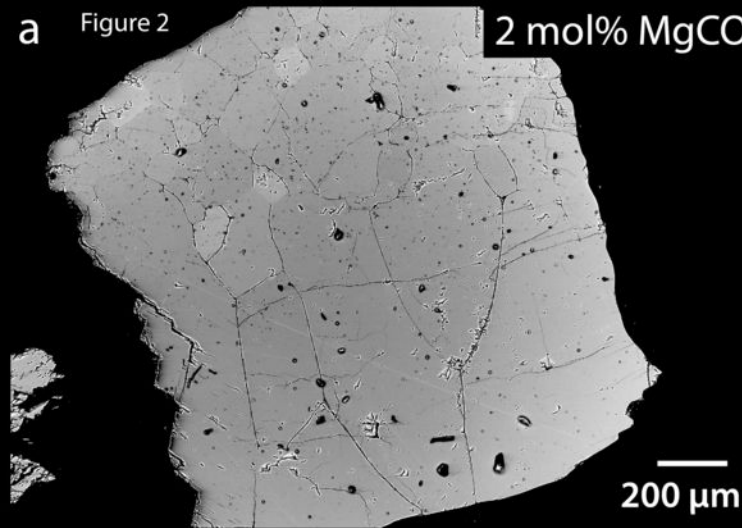
Valid in the range 0-50 mol% MgCO<sub>3</sub> except for  $\nu_1$  (0-30 mol% MgCO<sub>3</sub>). Note that for applications in the range 0-30 mol% MgCO<sub>3</sub>, equations presented in Table 4 should be preferred.

Figure 1



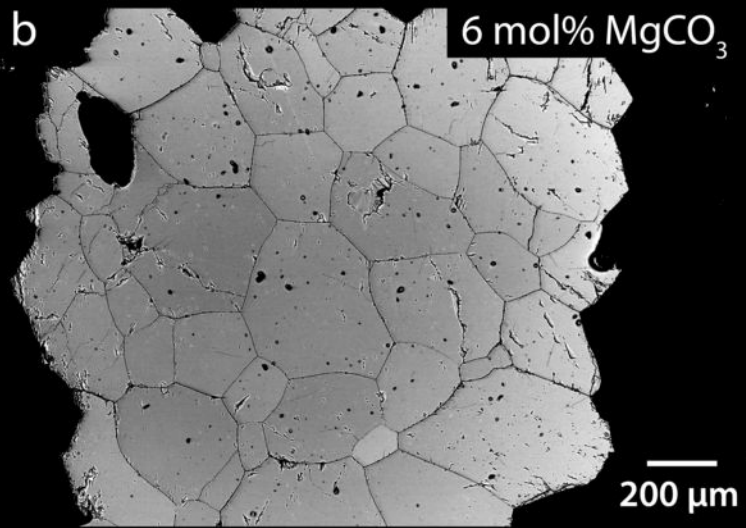
a Figure 2

2 mol%  $\text{MgCO}_3$



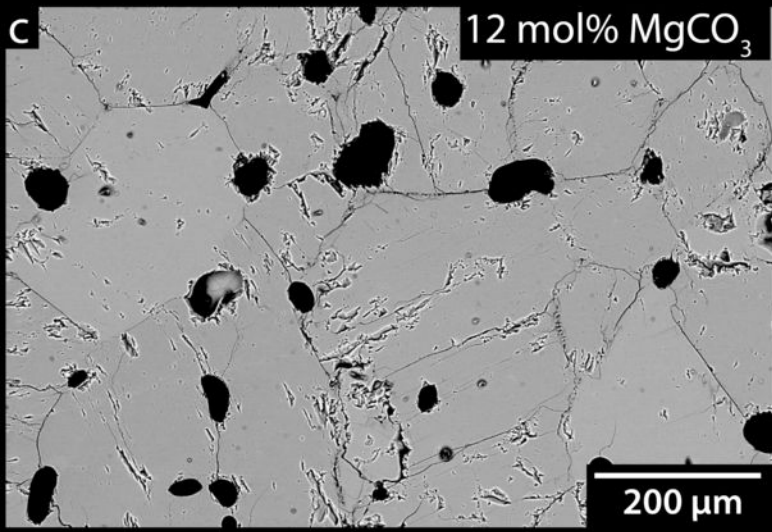
b

6 mol%  $\text{MgCO}_3$



c

12 mol%  $\text{MgCO}_3$



d

26 mol%  $\text{MgCO}_3$

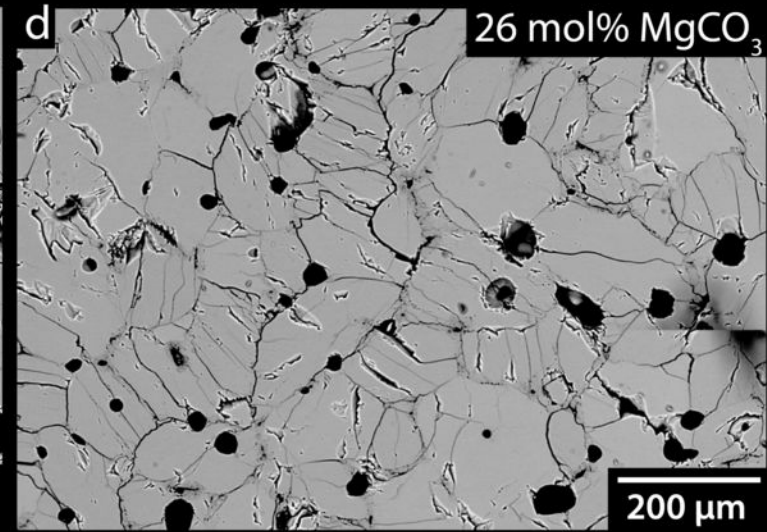
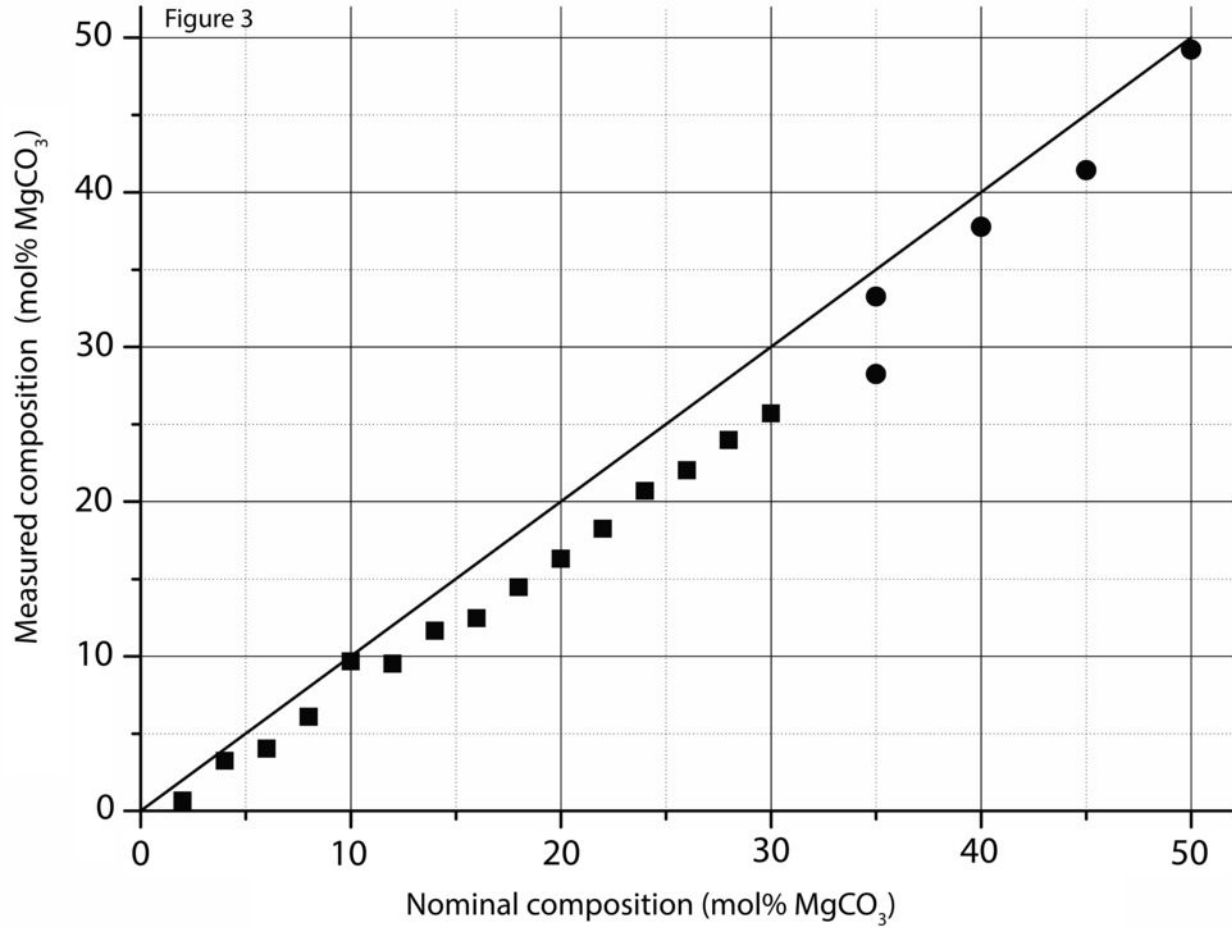
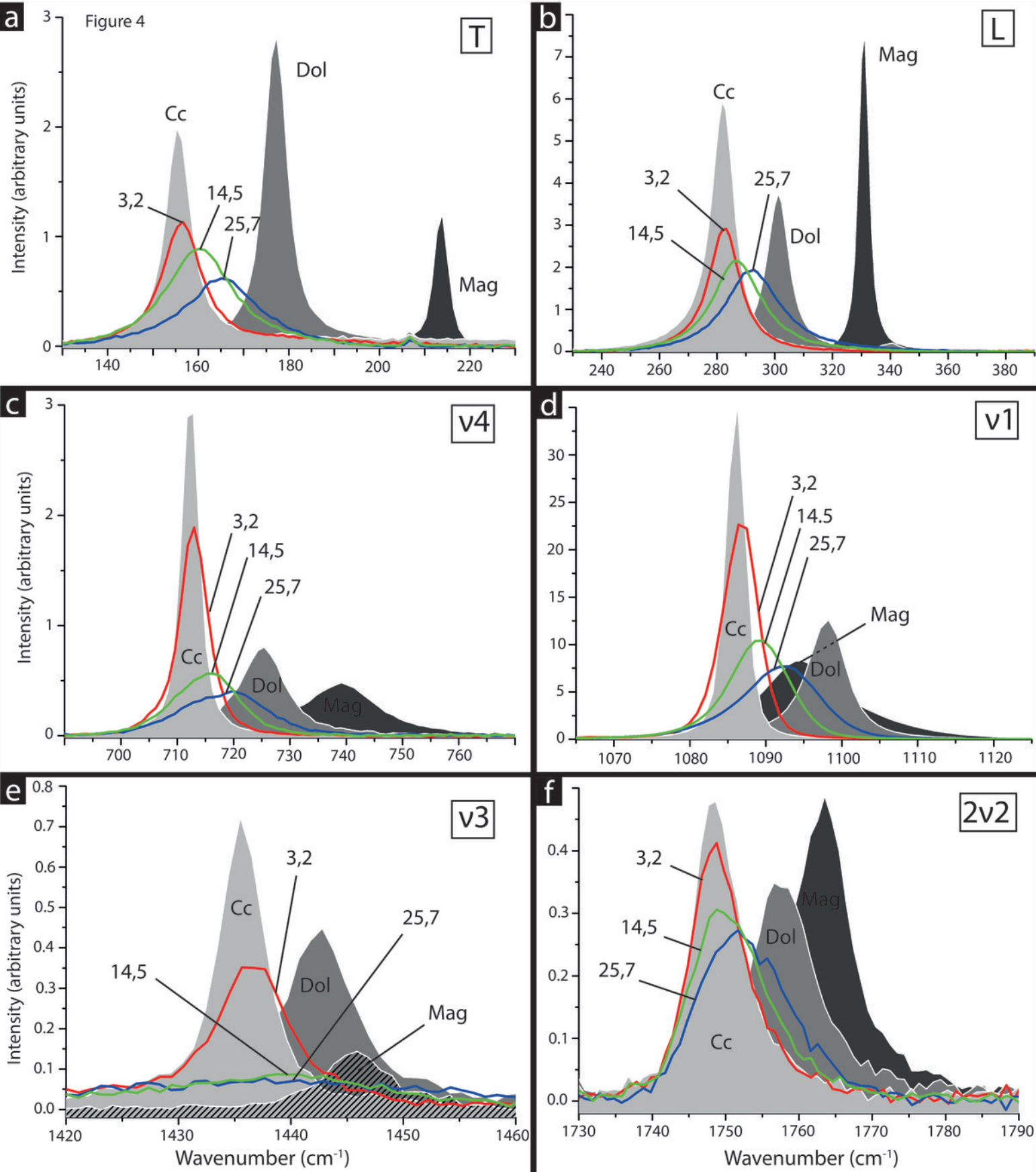
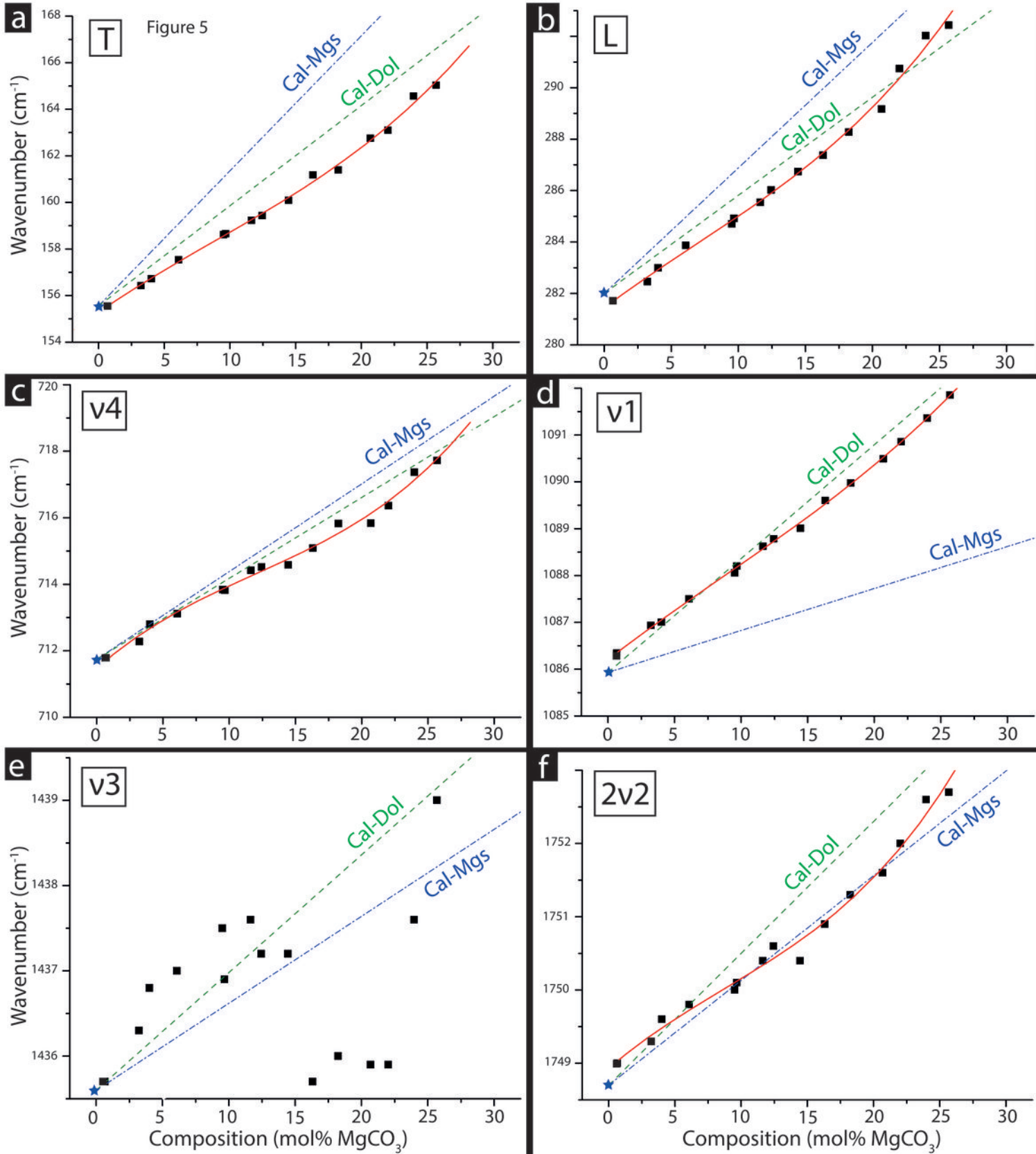


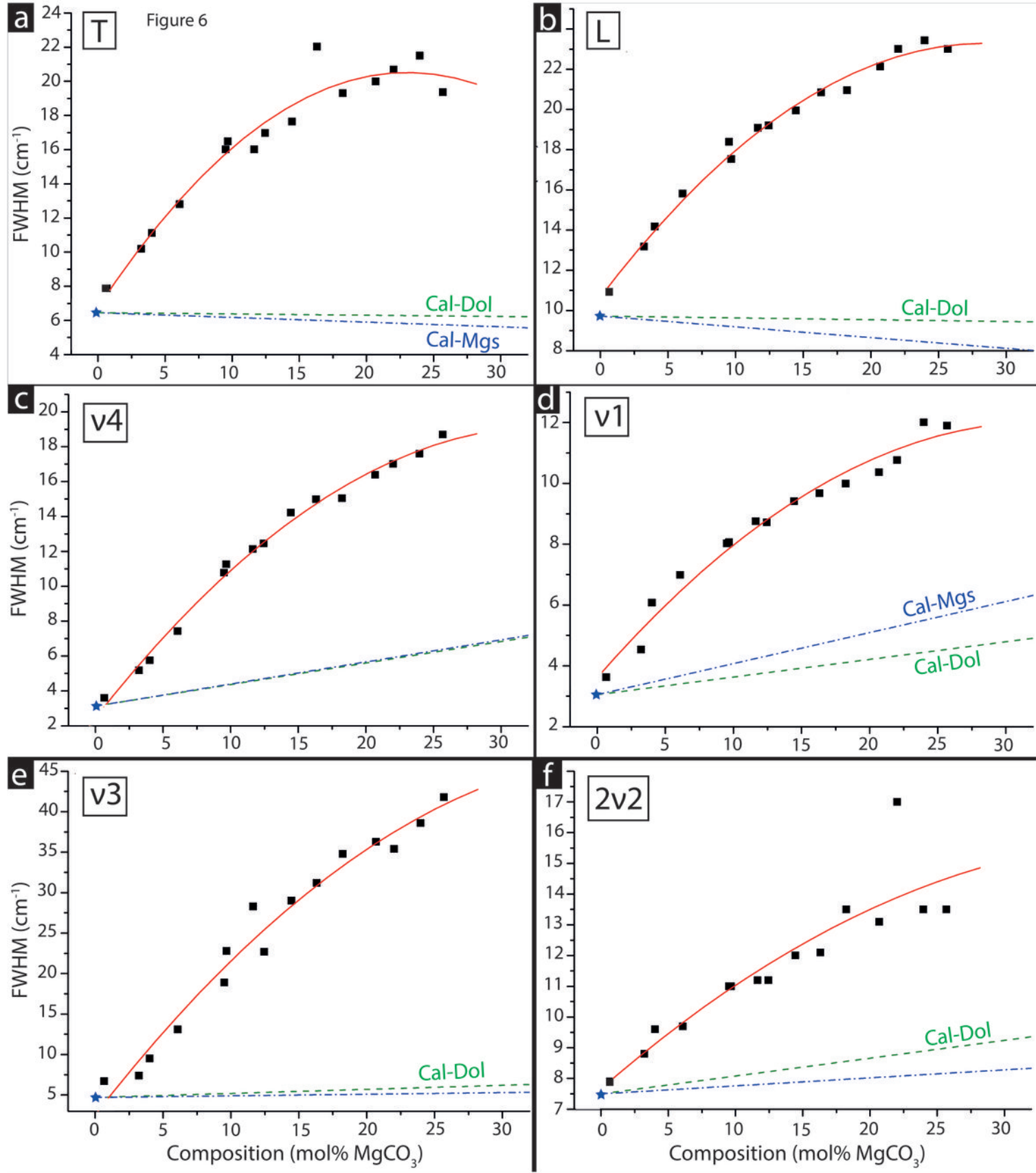
Figure 3

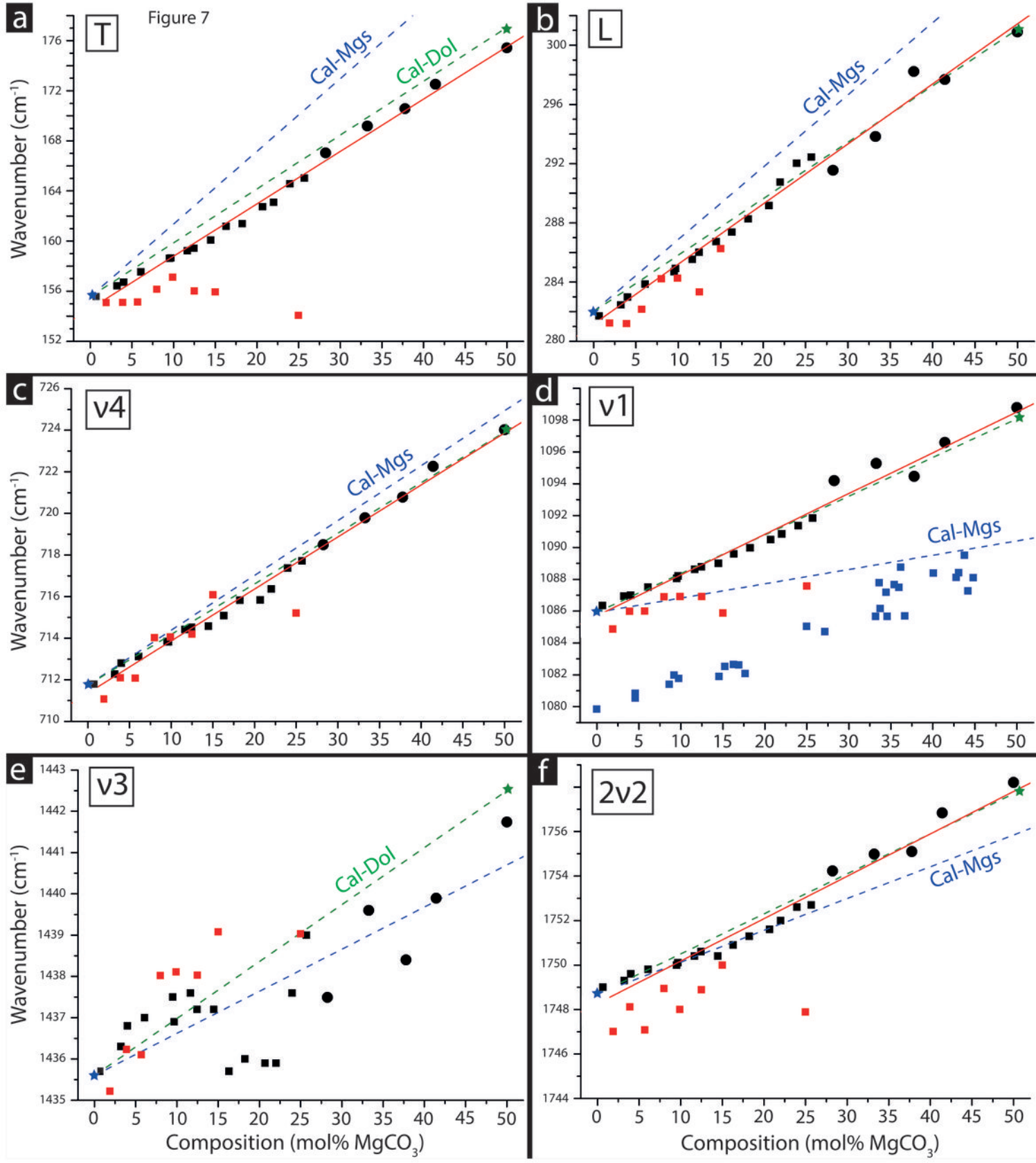












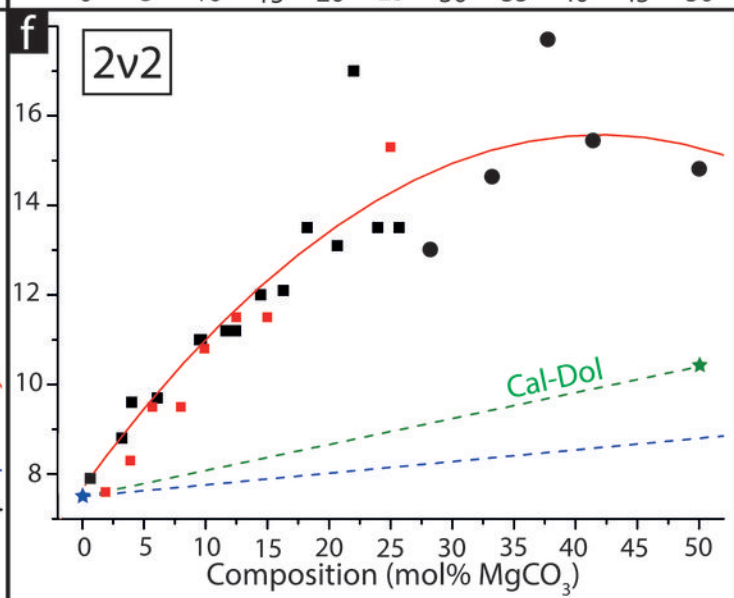
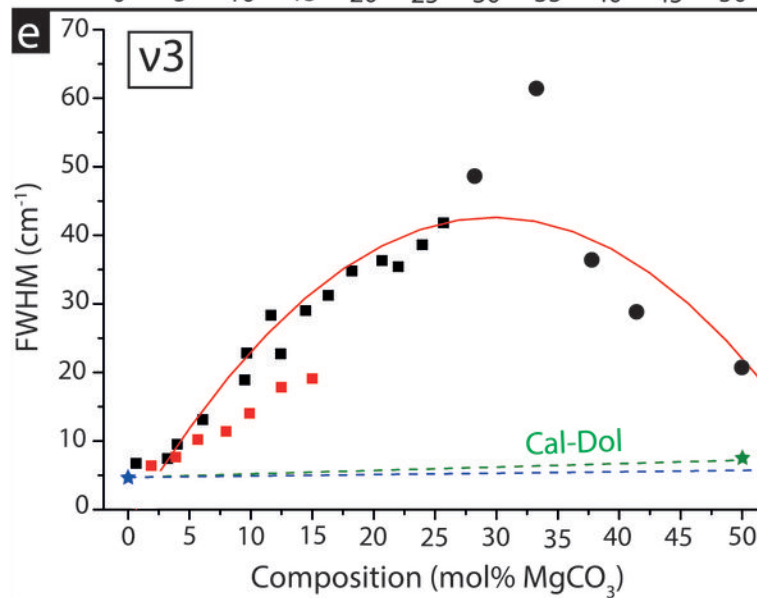
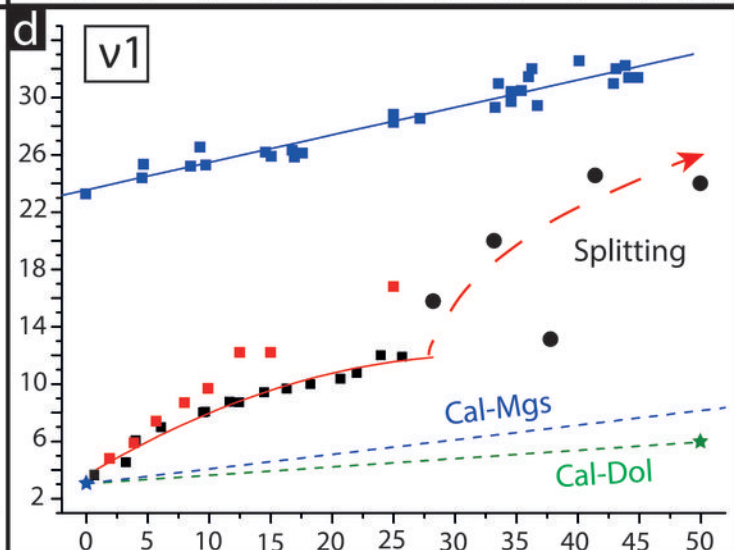
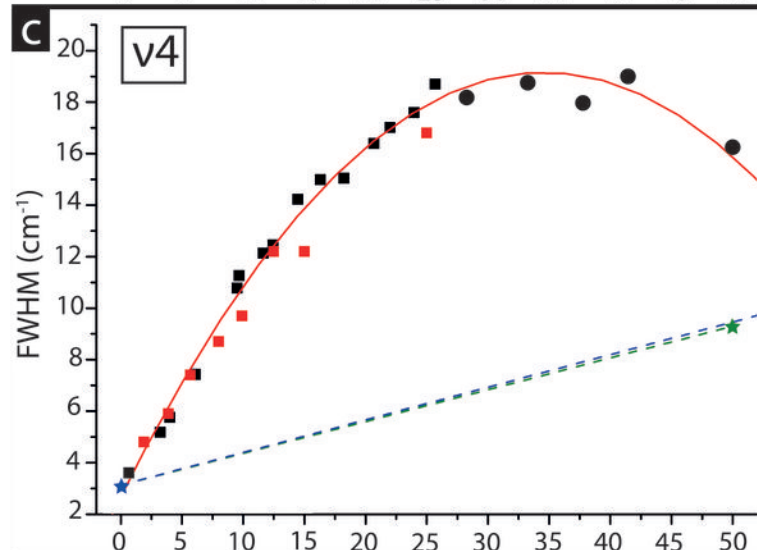
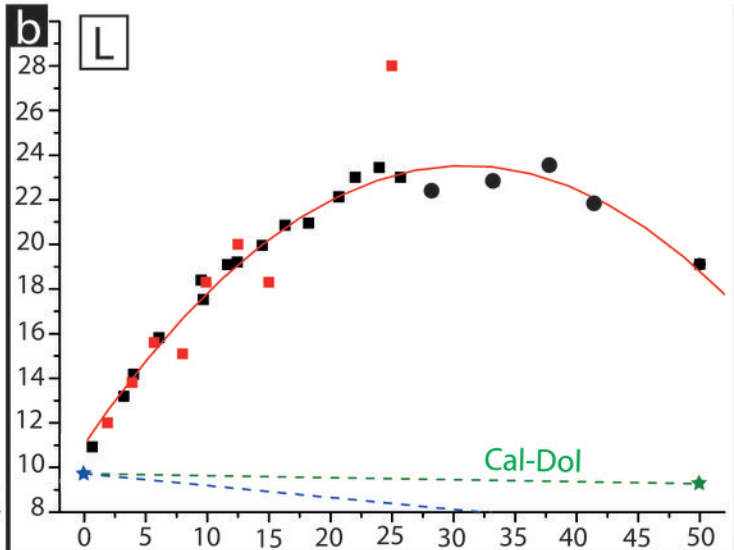
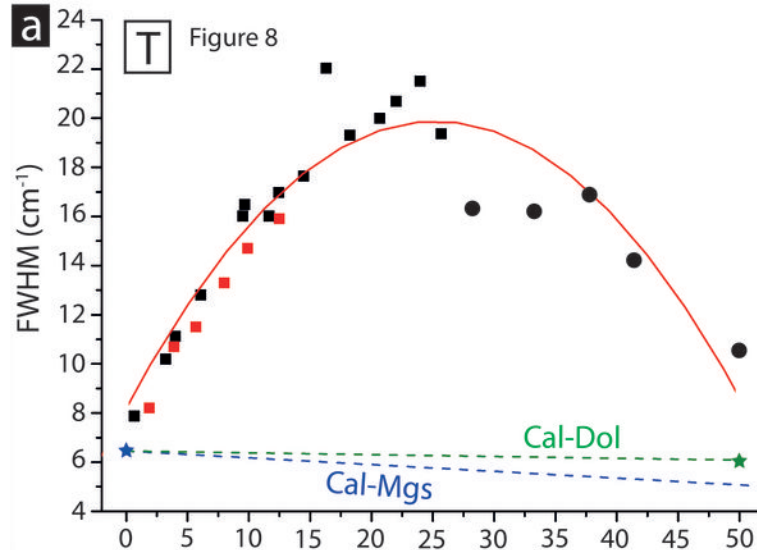
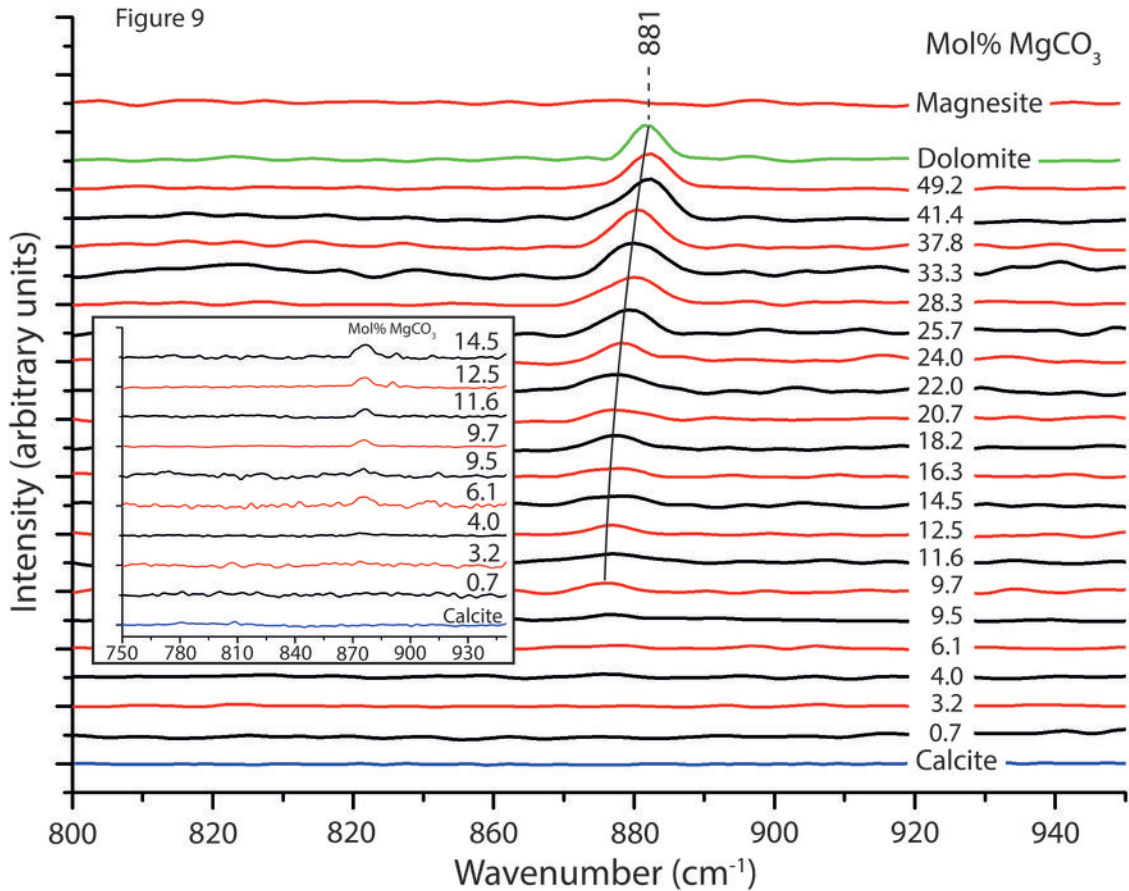
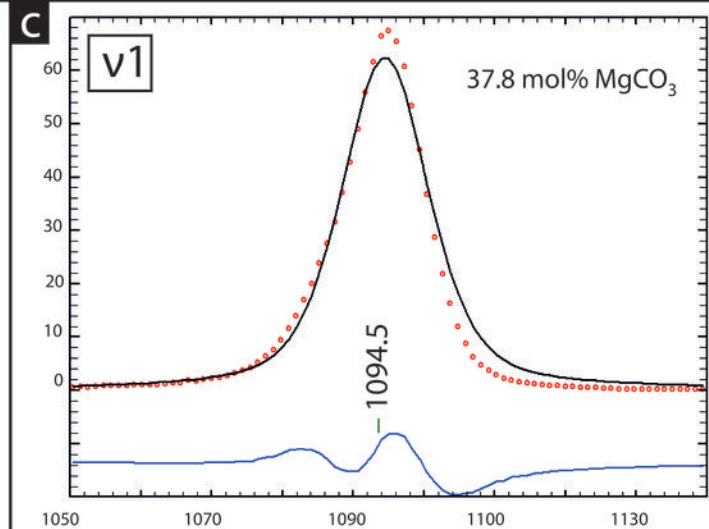
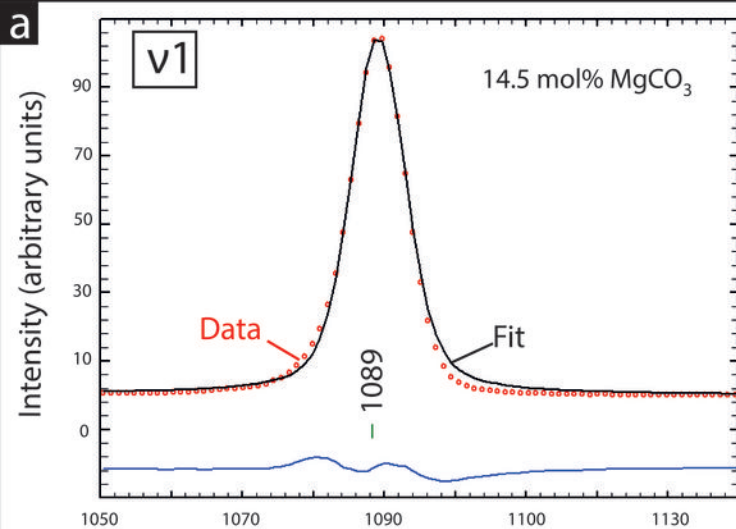


Figure 9





## Double peaks fitting

